J. Fluid Mech. (2022), *vol*. 935, A38, doi:10.1017/jfm.2022.37

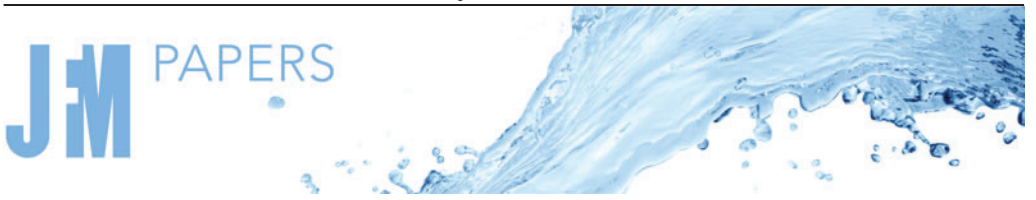

Transport coefficients for granular gases of electrically charged particles

Satoshi Takada[1],†, **Dan Serero**[2] **and Thorsten Pöschel**[2]

[1]Institute of Engineering, Tokyo University of Agriculture and Technology, 2-24-16, Naka-cho, Koganei, Tokyo 184-8588, Japan

[2]Lehrstuhl für Multiscale Simulation, Friedrich-Alexander-Universität Erlangen-Nürnberg, Cauerstraße 3, 91058 Erlangen, Germany

(Received 16 July 2021; revised 15 November 2021; accepted 10 January 2022)

We consider a dilute gas of electrically charged granular particles in the homogeneous cooling state. We derive the energy dissipation rate and the transport coefficients from the inelastic Boltzmann equation. We find that the deviation of the velocity distribution function from the Maxwellian yields overshoots of the transport coefficients, and especially, the negative peak of the Dufour-like coefficient, μ, in the intermediate granular temperature regime. We perform the linear stability analysis and investigate the granular temperature dependence of each mode, where the instability mode is found to change against the granular temperature. The molecular dynamics simulations are also performed to compare the result with that from the kinetic theory.

Key words: kinetic theory

1. Introduction

Dilute granular gases have been subject of intensive research in the past decades and by now there is a large body of knowledge regarding the fluid mechanical and kinetic properties of granular gases; see, e.g.Garzó (2019), Puglisi (2015), Brilliantov & Pöschel (2004), Goldhirsch (2003), Pöschel & Brilliantov (2003) and many references therein. There is an obvious similarity of ordinary molecular gases and granular gases which allows us to apply the mathematical toolbox of statistical physics and kinetic theory also to granular gases, however, modifications are needed to account for the loss of mechanical energy due to dissipative particle collisions. The irreversible transfer of energy from the mechanical degrees of freedom on the particle level to the thermal (sub-particular) degrees of freedom is characterized by the coefficient of restitution, e, defined as the ratio between the normal components of the pre-collisional and

† Email address for correspondence: takada@go.tuat.ac.jp

post-collisional relative velocities of the colliding grains. In the absence of external driving mechanisms, therefore, the kinetic energy of granular gases decays monotonously. For the case of a homogeneous granular gas and for a constant coefficient of restitution, this decay is described by Haff's law (Haff 1983) predicting decay of energy with time $\propto t^{-2}$. Similar results apply to gases of viscoelastic particles characterized by an impact velocity dependent coefficient of restitution (Brilliantov *et al.* 1996) where energy decays $\propto t^{-5/3}$ (Schwager & Pöschel 2008). The dissipative nature of particle interaction implies that granular gases are always in non-equilibrium, which gives rise to many interesting phenomena, such as non-Maxwellian velocity distribution (Goldhirsch, Noskowicz & Bar-Lev 2003), overpopulation of the high-energy tail of the velocity distribution function (Esipov & Pöschel 1997) or the instability of the homogeneous state in the long-time evolution (Goldhirsch & Zanetti 1993) which may be transient, depending on the particle characteristics (Brilliantov *et al.* 2004).

Much less is known when it comes to granular gases of electrically charged particles despite the fact that, for many applications of practical interest, it is known that electrical charges have significant influence or even dominate their macroscopic behaviour, e.g. Kumar *et al.* (2014), Laurentie, Traoré & Dascalescu (2013), Lee *et al.* (2015), Jungmann *et al.* (2018). Systems of charged particles – mostly due to triboelectricity – are not only ubiquitous in industrial processes (Kanazawa *et al.* 1995; Watanabe *et al.* 2007), but also in natural phenomena such as volcanic eruptions (Genareau *et al.* 2015) and in protoplanetary discs (Muranushi 2010). Although the triboelectric effect has been known since ancient times, the underlying physics is still the subject of intense scientific debate, e.g.Pan & Zhang (2019) and Lacks & Shinbrot (2019). Some recent work on this phenomenon can be found in Kolehmainen *et al.* (2016), Yoshimatsu *et al.* (2017), Singh & Mazza (2018) and Singh & Mazza (2019).

The presence of charges changes the collisional behaviour of granular particles significantly. For uncharged particles, the properties of a collision are independent of the unit of time. Particle interactions are instantaneous events resulting in a change of the particle velocities due to a collision rule. Independent of the incoming velocity, the absolute value of the relative particle velocity (in normal direction) reduces by a fraction described by the coefficient of restitution. This is different for charged particles. Here, a dissipative collision can only occur if the particles overcome an energy barrier induced by the electrical charges. In contrast to Haff's law, the kinetic energy decays $\propto \log^{-1}(t)$ rather than $\propto t^{-\alpha}$ (Scheffler & Wolf 2002). The same result with somewhat different reasoning was obtained by Pöschel, Brilliantov & Schwager (2003). For both results, a Maxwellian velocity distribution was assumed. While this assumption simplifies the algebra significantly, it ignores pronounced deviations from the Maxwellian as a consequence of inelastic collisions; see Goldshtein & Shapiro (1995), van Noije & Ernst (1998), Brey *et al.* (1998), Brilliantov & Pöschel (2000), Goldhirsch *et al.* (2003). When taking these deviations into account (Takada, Serero & Pöschel 2017), the functional form of the earlier result was reproduced, but the parameters and details are modified. That is, in the homogeneous cooling state of charged granular gases, initially the evolution of the granular temperature follows Haff's law (Haff 1983) followed by a later stage where the evolution follows the inverse of the logarithm of time.

In the current paper we continue the description of granular gases of charged particles by deriving the transport coefficients and, in particular, their dependence on granular temperature, especially in the discontinuous limit of the effective restitution coefficient. We expand our previous theory to the next order of the Sonine polynomial expansion of the velocity distribution function. We perform a linear stability analysis of the homogeneous

cooling state and find that the route to instability of a granular gas of charged particles differs from the route of uncharged particles. For a large granular temperature, the sound mode is stable and the heat mode is unstable for a small wavenumber, similar to granular gases of uncharged particles. For a small granular temperature, the heat mode becomes stable and the sound mode becomes unstable for a small wavenumber. This behaviour is not observed for uncharged gases. Instead, the shear mode is always dominant compared with the heat mode in the latter system (Brey *et al.* 1998; Brilliantov & Pöschel 2004).

For our analysis, we assume a dilute granular gas, that is, a small volume fraction of the particles. An extension to moderately dense systems would require an expression for the pair correlation function, which is however unknown for granular particles carrying charges.

In the next section we calculate the transport coefficients. In § 3 we perform the linear stability analysis for this system, and study the result in dependence on granular temperature. Finally, in § 4 we perform numerical simulations to validate the theoretical results. Some extensive calculations have been moved to the appendices so as not to disturb the flow of reading. In Appendix A we determine the Sonine coefficients a_2 and a_3 from the Boltzmann equation. Appendix B describes the derivation of Ω_η^e and Ω_κ^e needed for the transport coefficients. Finally, in Appendix C we explain the numerical method to compute the transport coefficients.

2. Kinetic theory and transport coefficients

2.1. *General method for the computation of transport coefficients*

We consider a system of charged monodisperse hard-sphere particles of mass m and diameter σ. For a small impact rate, charged particles interact elastically due to Coulomb's force law, while for a large rate, mechanical dissipative interaction dominates, characterized by a (constant) coefficient of restitution. Both regimes are separated by a critical rate v^*, depending on the values of mass and charge. The resulting step function, $e(v_n)$, is inconvenient for an analytical treatment, therefore, we chose a smooth step function $e(v_n, \beta)$ depending on a further parameter. Thus, our results will depend on this parameter β. The result concerning the step function is then obtained for $\beta \to \infty$. Following Takada *et al.* (2017), we describe the particle–particle interaction using the impact-rate dependent coefficient of restitution

$$e(v_n) = \frac{e^* \exp\left[\beta(v_n - v^*)\right] + 1}{\exp\left[\beta(v_n - v^*)\right] + 1}, \tag{2.1}$$

where v_n is the normal component of the relative velocity, v^* is a characteristic velocity and β is related to the slope of the change near v^* (see Takada *et al.* (2017), figure 1). The function (2.1) takes into account that, for $v_n \ll v^*$, the particles collide elastically, due to the repulsive charges. For $v_n \gg v^*$, the collision takes place as for uncharged particles, since inertia dominates the collision. Here, the coefficient of restitution assumes the value $e^* = \lim_{v_n/v^* \to \infty} e(v_n)$. For $\beta \to \infty$, we recover the step function used by Pöschel *et al.* (2003),

$$\lim_{\beta \to \infty} e(v_n) = 1 - \Theta(v_n - v^*)(1 - e^*), \tag{2.2}$$

where $\Theta(x)$ is the Heaviside function. In the homogeneous cooling state the granular temperature of the system decays due to inelastic collisions. This decay can be obtained

from the Boltzmann equation (Brilliantov & Pöschel 2004) as

$$\frac{\mathrm{d}T}{\mathrm{d}t} = -\frac{2}{3}n\sigma^2\sqrt{\frac{2T}{m}}\mu_2 T, \tag{2.3}$$

where n is the particle number density of the system and μ_2 is the second moment of the dimensionless collision integral. We expand the distribution function in terms of Sonine polynomials up to third order,

$$\tilde{f}(\boldsymbol{c}) = \phi(c)[1 + a_2 S_2(c^2) + a_3 S_3(c^2)], \tag{2.4}$$

where $\boldsymbol{c}$ is the dimensionless velocity $\boldsymbol{c} = \boldsymbol{v}/\sqrt{2T/m}$, $c = |\boldsymbol{c}|$, $\tilde{f}$ is the dimensionless velocity distribution function, $\phi(c)$ is the dimensionless Maxwell distribution function $\phi(c) = \pi^{-3/2}\exp(-c^2)$ and $S_p(x)$ $(p = 2, 3)$ are Sonine polynomials defined as (Brilliantov & Pöschel 2004; Chamorro, Reyes & Garzó 2013)

$$S_p(x) = \sum_{n=0}^{p} \frac{(-1)^n \left(\frac{1}{2} + p\right)!}{\left(\frac{1}{2} + n\right)!(p-n)!} x^p. \tag{2.5}$$

For μ_2, we obtain (Takada *et al.* 2017)

$$\mu_2 = \sqrt{2\pi}(S_1 + a_2 S_2 + a_3 S_3), \tag{2.6}$$

where the explicit forms of S_1, S_2 and S_3 are, respectively, given in Appendix A, (A5*a*)–(A5*c*). Similarly, we obtain the higher moments of the dimensionless collision integral

$$\mu_4 = \sqrt{2\pi}(T_1 + a_2 T_2 + a_3 T_3), \tag{2.7}$$

$$\mu_6 = \sqrt{2\pi}(D_1 + a_2 D_2 + a_3 D_3), \tag{2.8}$$

where T_1, T_2, T_3, D_1, D_2 and D_3 are, respectively, given in Appendix A, (A6*a*)–(A7*c*). Exploiting the properties of the collision integral, we can determine the coefficients a_2 and a_3 in linear approximation as

$$a_2 = \frac{N_2}{D}, \quad a_3 = \frac{N_3}{D}, \tag{2.9a,b}$$

with

$$N_2 \equiv (T_1 - 5S_1)\left(-\tfrac{105}{4}S_1 + \tfrac{105}{4}S_3 - D_3\right) - (5S_3 - T_3)\left(D_1 - \tfrac{105}{4}S_1\right), \tag{2.10a}$$

$$N_3 \equiv (5S_1 + 5S_2 - T_2)\left(D_1 - \tfrac{105}{4}S_1\right) - (T_1 - 5S_1)\left(\tfrac{315}{4}S_1 + \tfrac{105}{4}S_2 - D_2\right), \tag{2.10b}$$

$$D \equiv (5S_1 + 5S_2 - T_2)\left(-\tfrac{105}{4}S_1 + \tfrac{105}{4}S_3 - D_3\right) - (5S_3 - T_3)\left(\tfrac{315}{4}S_1 + \tfrac{105}{4}S_2 - D_2\right). \tag{2.10c}$$

(The detailed derivation is provided in Appendix A.)

Now, let us derive the transport coefficients where we follow the steps in Brilliantov & Pöschel (2003). Using the same procedure as the Chapman–Enskog method, we define

$$\Omega_\eta^e \equiv \int \mathrm{d}\boldsymbol{c}_1 \int \mathrm{d}\boldsymbol{c}_2 \int \mathrm{d}\hat{\boldsymbol{k}}\Theta(-\boldsymbol{c}_{12}\cdot\hat{\boldsymbol{k}})\left|\boldsymbol{c}_{12}\cdot\hat{\boldsymbol{k}}\right|\phi(c_1)\phi(c_2) \times [1 + a_2 S_2(c_1^2) + a_3 S_3(c_1^2)]\tilde{D}_{\alpha\beta}(\boldsymbol{c}_2)\Delta[\tilde{D}_{\alpha\beta}(\boldsymbol{c}_1) + \tilde{D}_{\alpha\beta}(\boldsymbol{c}_2)], \tag{2.11}$$

with (Brilliantov & Pöschel 2004)

$$\tilde{D}_{\alpha\beta}(\boldsymbol{c}) \equiv c_\alpha c_\beta - \tfrac{1}{3}c^2\delta_{\alpha\beta}. \tag{2.12}$$

Greek characters $\{\alpha, \beta\}$ stand for $\{x, y, z\}$, and we adopt Einstein's rule for the summation. We have also introduced $\Delta\psi(\boldsymbol{c}_i) \equiv \psi(\boldsymbol{c}_i') - \psi(\boldsymbol{c}_i)$ for an arbitrary function ψ (Brilliantov & Pöschel 2004). Substituting (2.1) into (2.11), we obtain

$$\Omega_\eta^e = \sqrt{2\pi}(\omega_{\eta,1}^e + a_2\omega_{\eta,2}^e + a_3\omega_{\eta,3}^e), \tag{2.13}$$

where $\Omega_{\eta,1}^e$, $\Omega_{\eta,2}^e$ and $\Omega_{\eta,3}^e$ are, respectively, given in Appendix B, (B5*a*)–(B5*c*).

Similarly, we define

$$\Omega_\kappa^e \equiv \int \mathrm{d}\boldsymbol{c}_1 \int d\boldsymbol{c}_2 \int \mathrm{d}\hat{\boldsymbol{k}}\Theta(-\boldsymbol{c}_{12}\cdot\hat{\boldsymbol{k}})\left|\boldsymbol{c}_{12}\cdot\hat{\boldsymbol{k}}\right|\phi(c_1)\phi(c_2) \times [1 + a_2 S_2(c_1^2) + a_3 S_3(c_1^2)]\tilde{\boldsymbol{S}}(\boldsymbol{c}_2)\Delta[\tilde{\boldsymbol{S}}(\boldsymbol{c}_1) + \tilde{\boldsymbol{S}}(\boldsymbol{c}_2)], \tag{2.14}$$

with (Brilliantov & Pöschel 2004)

$$\tilde{\boldsymbol{S}}(\boldsymbol{c}) \equiv \left(c^2 - \tfrac{5}{2}\right)\boldsymbol{c}. \tag{2.15}$$

We obtain

$$\Omega_\kappa^e = \sqrt{2\pi}(\omega_{\kappa,1}^e + a_2\omega_{\kappa,2}^e + a_3\omega_{\kappa,3}^e), \tag{2.16}$$

where $\Omega_{\kappa,1}^e$, $\Omega_{\kappa,2}^e$ and $\Omega_{\kappa,3}^e$ are, respectively, given in Appendix B, (B8*a*)–(B8*c*).

2.2. *Discontinuous limit of the restitution coefficient*

Consider the transport coefficients in the discontinuous limit, $\beta v^* \to \infty$. In this limit, (2.6)–(2.8), (2.13) and (2.16) read as

$$\mu_2^{(\infty)} = \sqrt{2\pi}\left(S_1^{(\infty)} + a_2^{(\infty)}S_2^{(\infty)} + a_3^{(\infty)}S_3^{(\infty)}\right), \tag{2.17a}$$

$$\mu_4^{(\infty)} = \sqrt{2\pi}\left(T_1^{(\infty)} + a_2^{(\infty)}T_2^{(\infty)} + a_3^{(\infty)}T_3^{(\infty)}\right), \tag{2.17b}$$

$$\mu_6^{(\infty)} = \sqrt{2\pi}\left(D_1^{(\infty)} + a_2^{(\infty)}D_2^{(\infty)} + a_3^{(\infty)}D_3^{(\infty)}\right), \tag{2.17c}$$

$$\Omega_\eta^{e(\infty)} = \sqrt{2\pi}\left(\omega_{\eta,1}^{e(\infty)} + a_2^{(\infty)}\omega_{\eta,2}^{e(\infty)} + a_3^{(\infty)}\omega_{\eta,3}^{e(\infty)}\right), \tag{2.17d}$$

$$\Omega_\kappa^{e(\infty)} = \sqrt{2\pi}\left(\omega_{\kappa,1}^{e(\infty)} + a_2^{(\infty)}\omega_{\kappa,2}^{e(\infty)} + a_3^{(\infty)}\omega_{\kappa,3}^{e(\infty)}\right), \tag{2.17e}$$

whose explicit forms are given in Appendices A and B. Hereafter, we focus on the discontinuous limit $\beta v^* \to \infty$; we drop the superscript (∞) for simplicity.

Let us start with the coefficients a_2 and a_3. Figure 1 shows a_2 and a_3 as functions of granular temperature given by (2.9*a*,*b*) in the limit $\beta v^* \to \infty$. In the figure we have introduced the characteristic granular temperature, $T^* \equiv m v^{*2}/2$, given by the characteristic rate v^* (Takada *et al.* 2017). We also show a_2 as obtained when the third term in (2.4) is neglected, that is, with the assumption $a_3 = 0$. The explicit form of a_2 with $a_3 = 0$ is given in Takada *et al.* (2017, equation (10)). For a high granular temperature, we obtain $\lim_{T\to\infty} a_2(T) = a_2^{(HC)}$ and $\lim_{T\to\infty} a_3(T) = a_3^{(HC)}$, where $a_2^{(HC)}$ and $a_3^{(HC)}$ are the Sonine coefficients for a gas of hard spheres (Brilliantov & Pöschel 2006),

$$a_2^{(HC)}(e^*) \equiv \frac{N_2^{(HC)}(e^*)}{D^{(HC)}(e^*)}, \tag{2.18a}$$

$$a_3^{(HC)}(e^*) \equiv \frac{N_3^{(HC)}(e^*)}{D^{(HC)}(e^*)}, \tag{2.18b}$$

with

$$\begin{aligned} N_2^{(HC)}(e^*) \equiv 16\Big(&1623 - 1934e^* - 895e^{*2} + 364e^{*3} - 3510e^{*4} \\ &+7424e^{*5} - 3312e^{*6} + 480e^{*7} - 240e^{*8}\Big), \end{aligned} \tag{2.19a}$$

$$\begin{aligned} N_3^{(HC)}(e^*) \equiv -128\Big(&217 - 386e^* - 669e^{*2} + 1548e^{*3} + 154e^{*4} \\ &-1600e^{*5} + 816e^{*6} - 160e^{*7} + 80e^{*8}\Big), \end{aligned} \tag{2.19b}$$

$$\begin{aligned} D^{(HC)}(e^*) \equiv\ &214\,357 - 172\,458e^* + 112\,155e^{*2} + 25\,716e^{*3} - 4410e^{*4} \\ &- 84\,480e^{*5} + 34\,800e^{*6} - 5600e^{*7} + 2800e^{*8}. \end{aligned} \tag{2.19c}$$

The coefficient a_3 has both a minimum and maximum in the intermediate regime, while a_2 has only a minimum in this regime. The position of the minimum of a_3 coincides almost with the position of the minimum of a_2. From (2.3), the dissipation rate ζ is written as

$$\zeta = \frac{2}{3} n\sigma^2 \sqrt{\frac{2T}{m}}\mu_2. \tag{2.20}$$

Figure 2 shows the dissipation rate as a function of granular temperature. Here, we introduce a new variable

$$\zeta^* \equiv \frac{\zeta}{\zeta^{(HC)}(e^*)}, \tag{2.21}$$

where

$$\zeta^{(HC)}\left(e^*\right) = \frac{4}{3}\left(1 - e^{*2}\right) n\sigma^2 \sqrt{\frac{\pi T}{m}}\mu_2^{(HC)}\left(1 + \frac{3}{16}a_2^{(HC)}\left(e^*\right) + \frac{1}{64}a_3^{(HC)}\left(e^*\right)\right). \tag{2.22}$$

In the limit of high granular temperature, the dissipation rate is consistent with the hard-sphere limit while it decreases to zero as the granular temperature becomes sufficiently smaller than the characteristic granular temperature.

Next, we consider the shear viscosity, η, as a function of granular temperature, using the technique introduced in Takada, Saitoh & Hayakawa (2016). Then, the shear viscosity is

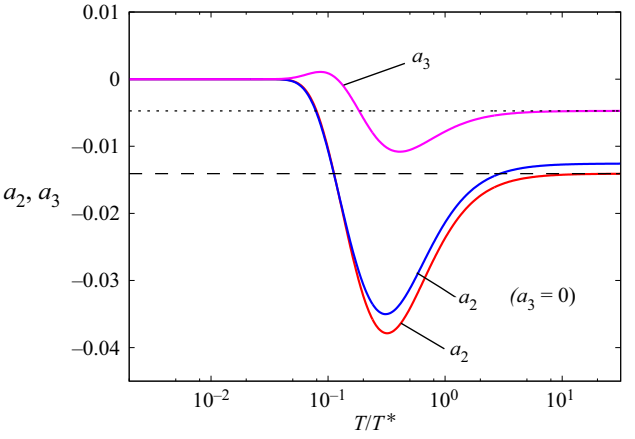

Figure 1. The coefficients a_2 and a_3 as functions of the granular temperature for $e^* = 0.8$. For the computation of the blue curve, we neglected a_3 in (2.4), that is, $a_3 = 0$ was assumed. The explicit form of $a_2(T)$ with $a_3 = 0$ is given by (2.18).

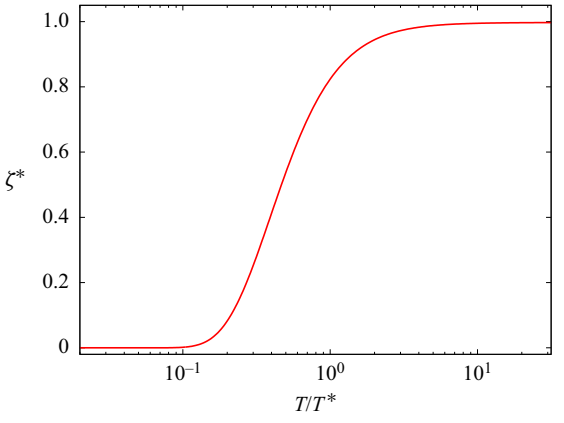

Figure 2. Dissipation rate as a function of granular temperature, obtained from the kinetic theory up to order a_3 for $e^* = 0.8$, where ζ^* is given by (2.21).

given by the solution of the differential equation

$$-\frac{2}{3}T\mu_2\frac{\partial\eta}{\partial T} - \frac{2}{5}\Omega_\eta^e\eta = \frac{1}{\sigma^2}\sqrt{\frac{mT}{2}}. \tag{2.23}$$

Here, we define a new variable

$$\eta^* \equiv \frac{\eta}{\eta^{(HC)}(1)}, \quad \text{where } \eta^{(HC)}(1) = \frac{5}{16\sigma^2}\sqrt{\frac{mT}{\pi}} \tag{2.24}$$

is the shear viscosity of the elastic hard-sphere gas. Using η^*, (2.23) reads as

$$10x\mu_2\frac{\partial\eta^*}{\partial x} - (5\mu_2 + 6\Omega_\eta^e)\eta^* = 24\sqrt{2\pi}; \quad x \equiv \frac{T^*}{2T}. \tag{2.25a,b}$$

To solve this equation perturbatively, we expand $\eta^* = \eta^{*(0)} + \eta^{*(1)} + \dots$ and assume that the first term on the left-hand side of (2.25*a*,*b*) is of higher order than the other terms.

For justification and discussion of this assumption, see § 5. Then we can perturbatively solve (2.25*a*,*b*). To this end, we expand the viscosity $\eta^* = \eta^{*(0)} + \varepsilon\eta^{*(1)} + \dots$, where ε is a perturbative parameter relating to the inelasticity $(1 - e^{*2})$. Since μ_2 corresponds to the energy dissipation rate, $\mu_2 \sim O(\varepsilon)$. Using these assumptions, (2.25*a*,*b*) is rewritten as

$$10x\varepsilon\mu_2\frac{\partial}{\partial x}(\eta^{*(0)} + \varepsilon\eta^{*(1)} + \dots) - (5\mu_2 + 6\Omega_\eta^e)(\eta^{*(0)} + \varepsilon\eta^{*(1)} + \dots) = 24\sqrt{2\pi}. \tag{2.26}$$

Collecting terms in each order and setting $\varepsilon = 1$, we obtain

$$\eta^* = \sum_{n=0}^{\infty}\eta^{*(n)} = \sum_{n=0}^{\infty}\left(\frac{10x\mu_2}{5\mu_2 + 6\Omega_\eta^e}\frac{\partial}{\partial x}\right)^n \eta^{*(0)}, \tag{2.27}$$

with

$$\eta^{*(0)} = -\frac{24\sqrt{2\pi}}{5\mu_2 + 6\Omega_\eta^e}. \tag{2.28}$$

Note that

$$\frac{\partial}{\partial x} = -\frac{2T^2}{T^*}\frac{\partial}{\partial T} \tag{2.29}$$

holds true. Figure 3 shows the shear viscosity as a function of granular temperature, (2.27), up to the first order. In the limit of high granular temperature, we recover the result for an inelastic hard-sphere gas while, for a low granular temperature, we find the result for the elastic hard-sphere gas. This agrees with the intuition that, for a high granular temperature, nearly all collisions are dissipative while, for a low granular temperature, elastic collisions dominate. In the intermediate region we obtain a negative overshoot around $T/T^* \simeq 0.1$. This behaviour is also observed when we assume a Maxwell distribution function (not shown in figure 3). We also show the numerical solution of the differential equation (2.25*a*,*b*); details are discussed in Appendix C. The numerical result is consistent with the perturbative solution, that is, the numerics support the validity of the theoretical result.

Similarly, the thermal conductivity and the Dufour-like coefficient μ (see Garzó 2019; Shukla, Biswas & Gupta 2019; Gupta, Shukla & Torrilhon 2020) are, respectively, given by the solutions of the differential equations

$$\frac{\partial}{\partial T}\left(4\mu_2\kappa T^{3/2}\right) + \frac{8}{5}\kappa T^{1/2}\Omega_\kappa^e = -\frac{15}{2}\frac{T}{\sigma^2}\sqrt{\frac{2}{m}}(1 + 2a_2), \tag{2.30}$$

$$-4\mu_2\frac{\partial\mu}{\partial T} - \frac{8}{5}T^{-1}\Omega_\kappa^e\mu = \frac{4}{n}\mu_2\kappa + a_2\frac{15}{2n\sigma^2}\sqrt{\frac{2T}{m}}. \tag{2.31}$$

Introducing new variables

$$\kappa^* \equiv \frac{\kappa}{\kappa^{(HC)}(1)} \quad \text{and} \quad \mu^* = \frac{\frac{n\mu}{T}}{\kappa^{(HC)}(1)} \tag{2.32a,b}$$

with the thermal conductivity of the elastic hard-sphere gas

$$\kappa^{(HC)}(1) = \frac{75}{64\sigma^2}\sqrt{\frac{T}{\pi m}}, \tag{2.33}$$

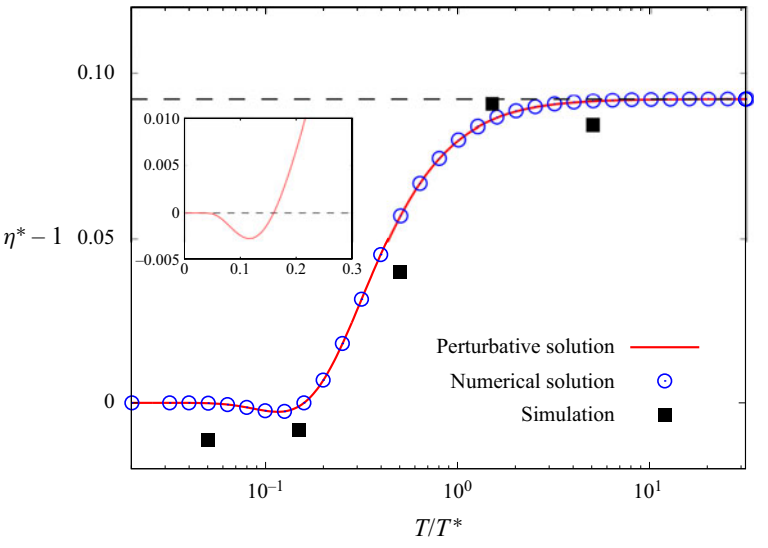

Figure 3. Shear viscosity as a function of granular temperature obtained from the kinetic theory perturbatively (solid line) and numerically as discussed in Appendix C (open circles) for $e^* = 0.8$, where η^* is given by (2.24). The filled squares show results obtained from an event-driven molecular dynamics simulation. The dashed line is the shear viscosity of a hard-sphere gas, $\eta^{(HC)}(e^*)/\eta^{HC}(1)$, (C1). The inset shows a magnification of the intermediate regime.

we can rewrite (2.30) and (2.31),

$$5x\mu_2\frac{\partial\kappa^*}{\partial x}-\left(10\mu_2-5x\frac{\partial\mu_2}{\partial x}+2\Omega_\kappa^e\right)\kappa^*=8\sqrt{2\pi}(1+2a_2), \tag{2.34}$$

$$10x\mu_2\frac{\partial\mu^*}{\partial x}-\left(15\mu_2+4\Omega_\kappa^e\right)\mu^*=2\mu_2\kappa^*+16\sqrt{2\pi}a_2. \tag{2.35}$$

Similar to the shear viscosity, we can perturbatively obtain the solutions as

$$\kappa^*=\sum_{n=0}^{\infty}\kappa^{*(n)}=\sum_{n=0}^{\infty}\left(\frac{5x\mu_2}{10\mu_2-5x\mu_2'+2\Omega_\kappa^e}\frac{\partial}{\partial x}\right)^n\kappa^{*(0)}, \tag{2.36}$$

$$\mu^*=\sum_{n=0}^{\infty}\mu^{*(n)}=\sum_{n=0}^{\infty}\left(\frac{10x\mu_2}{15\mu_2+4\Omega_\kappa^e}\frac{\partial}{\partial x}\right)^n\mu^{*(0)}, \tag{2.37}$$

respectively, with

$$\mu_2'=\frac{\partial\mu_2}{\partial x}, \tag{2.38}$$

$$\kappa^{*(0)}=-\frac{8\sqrt{2\pi}(1+2a_2)}{10\mu_2-5x\mu_2'+2\Omega_\kappa^e}, \tag{2.39}$$

$$\mu^{*(0)}=-\frac{10\mu_2\kappa^*+16\sqrt{2\pi}a_2}{15\mu_2+4\Omega_\kappa^e}. \tag{2.40}$$

Figures 4 and 5 show the thermal conductivity, (2.36), and the Dufour-like coefficient μ, (2.37), as functions of granular temperature. Again, the numerical solution supports the validity of the analytical results.

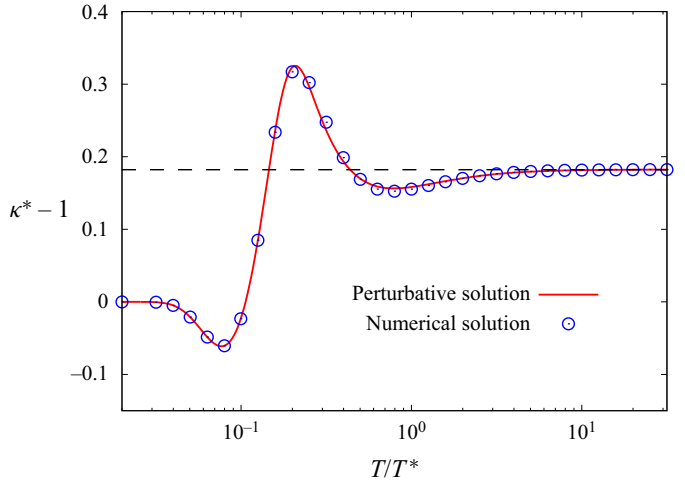

Figure 4. Thermal conductivity as a function of granular temperature, obtained from the kinetic theory perturbatively (solid line) and numerically as discussed in Appendix C (open circles) for $e^* = 0.8$, where κ^* is given by (2.32*a*,*b*). The dashed line is the thermal conductivity of a hard-sphere gas $\kappa^{(HC)}(e^*)/\kappa^{(HC)}(1)$ (C 7).

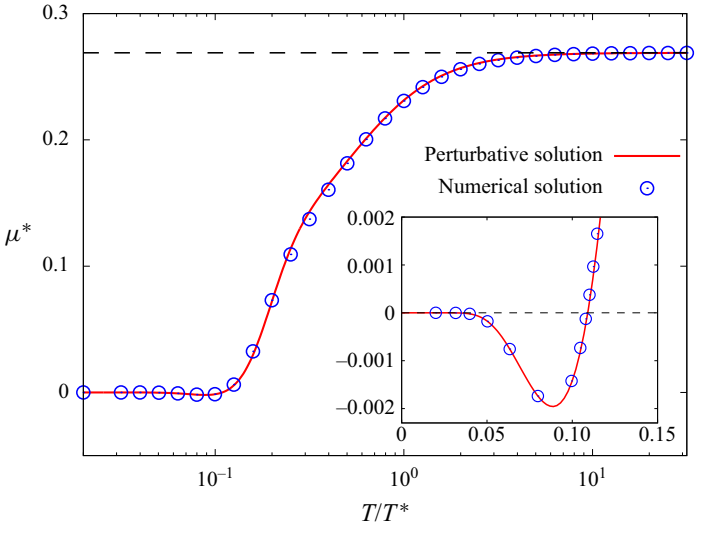

Figure 5. The granular temperature dependence of the Dufour-like coefficient μ obtained from the kinetic theory perturbatively (solid line) and numerically as discussed in Appendix C (open circles) for $e^* = 0.8$, where μ^* is given by (2.32*a*,*b*). The dashed line shows the result for an inelastic hard-sphere gas, $n\mu^{(HC)}(e^*)/(\kappa^{(HC)}(1)T)$ (C9). The inset shows a magnification of the intermediate regime.

The thermal conductivity has both negative and positive peaks at around $T/T^* \simeq 0.1$ and 0.2, respectively. Similar to the case of the shear viscosity, these peaks are not found when a Maxwell distribution function is assumed. The Dufour-like coefficient μ behaves similar to the shear viscosity, however, the value becomes negative in this region as shown in the inset of figure 5. This means that the heat flux is directed from dilute regions to dense regions. We will discuss this phenomenon below.

3. Linear stability analysis of the homogeneous cooling state

From the zeroth, first and second moments of the Boltzmann equation, we obtain a set of hydrodynamic equations,

$$\frac{\partial n}{\partial t} + \boldsymbol{\nabla}\cdot(n\boldsymbol{u}) = 0, \tag{3.1a}$$

$$\frac{\partial \boldsymbol{u}}{\partial t} + \boldsymbol{u}\cdot\boldsymbol{\nabla}\boldsymbol{u} = -\frac{1}{nm}\boldsymbol{\nabla}p + \frac{\eta}{nm}\left[\nabla^2\boldsymbol{u} + \frac{1}{3}\boldsymbol{\nabla}(\boldsymbol{\nabla}\cdot\boldsymbol{u})\right], \tag{3.1b}$$

$$\begin{aligned}\frac{\partial T}{\partial t} + \boldsymbol{u}\cdot\boldsymbol{\nabla}T = -\zeta T + \frac{2}{3n}\left(\kappa\nabla^2 T + \mu\nabla^2 n\right) - \frac{2}{3n}p(\boldsymbol{\nabla}\cdot\boldsymbol{u}) \\ + \frac{2}{3n}\eta\left[(\nabla_\alpha u_\beta)(\nabla_\beta u_\alpha) + (\nabla_\beta u_\alpha)(\nabla_\alpha u_\beta) - \frac{2}{3}(\boldsymbol{\nabla}\cdot\boldsymbol{u})^2\right],\end{aligned} \tag{3.1c}$$

with the static pressure $p = nT$. We linearize the equations around the homogeneous cooling state,

$$n(\boldsymbol{r}, t) = n_H + \delta n, \tag{3.2a}$$

$$T(\boldsymbol{r}, t) = T_H + \delta T, \tag{3.2b}$$

where the subscript H indicates the quantities due to the homogeneous system and consider only linear terms with respect to

$$\rho \equiv \frac{\delta n}{n_H}, \quad \boldsymbol{w} \equiv \frac{\boldsymbol{u}}{v_T}, \quad \theta \equiv \frac{\delta T}{T_H}, \tag{3.3a–c}$$

with the thermal velocity $v_T \equiv \sqrt{2T/m}$. We introduce dimensionless time and space variables, τ and $\hat{\boldsymbol{r}}$, by

$$\tau \equiv \int_0^t \mathrm{d}t' v_H(t'), \tag{3.4a}$$

$$\hat{\boldsymbol{r}} \equiv \frac{2v_H(t)}{v_T(t)}\boldsymbol{r}, \tag{3.4b}$$

with the collision frequency for the elastic hard-sphere gas

$$v_H = \frac{16}{5}n\sigma^2\sqrt{\frac{\pi T}{m}}. \tag{3.5}$$

After linearization and Fourier transformation, the set of hydrodynamic equations becomes

$$\frac{\partial}{\partial\tau}\rho_k = -\mathrm{i}kw_{k\parallel}, \tag{3.6a}$$

$$\frac{\partial}{\partial\tau}w_{k\parallel} = -\frac{1}{2}\mathrm{i}k\rho_k + \left(\frac{1}{4}\zeta^* - \frac{4}{3}\eta^* k^2\right)w_{k\parallel} - \frac{1}{2}\mathrm{i}k\theta_k, \tag{3.6b}$$

$$\frac{\partial}{\partial\tau}w_{k\perp} = \left(\frac{1}{4}\zeta^* - \eta^* k^2\right)w_{k\perp}, \tag{3.6c}$$

$$\frac{\partial}{\partial\tau}\theta_k = \left(-\frac{1}{2}\zeta^* - \frac{5}{2}\mu^* k^2\right)\rho_k - \frac{2}{3}\mathrm{i}kw_{k\parallel} + \left(-A\zeta^* - \frac{5}{2}\kappa^* k^2\right)\theta_k, \tag{3.6d}$$

with

$$\zeta^* = \zeta \frac{\eta^{(HC)}(1)}{nT} \tag{3.7}$$

and

$$A \equiv \frac{1}{4} + \frac{1}{2} T \frac{\partial}{\partial T} \log \mu_2 = \frac{1}{4} - \frac{1}{2} x \frac{\partial}{\partial x} \log \mu_2. \tag{3.8}$$

In the limit $x \to 0$ we obtain $A \to 1/4$, which is consistent with the result for hard-sphere gases (Brilliantov & Pöschel 2004). The variables $\Psi_k (= \rho_k, \boldsymbol{w}_k, \theta_k)$ denote the Fourier component of the quantity Ψ,

$$\Psi_k(\tau) = \int \mathrm{d}\,\hat{\boldsymbol{r}} \Psi(\hat{\boldsymbol{r}}, \tau) \mathrm{e}^{-\mathrm{i}\boldsymbol{k}\cdot\hat{\boldsymbol{r}}} \tag{3.9}$$

and $w_{\boldsymbol{k}\parallel}$ and $\boldsymbol{w}_{\boldsymbol{k}\perp}$ are the longitudinal and transversal components of the velocity field with respect to the dimensionless wave vector $\boldsymbol{k}$.

Equation (3.6*c*) can be easily solved as

$$w_{k\perp}(\tau) = w_{k\perp}(0) \exp(\lambda_\perp \tau), \tag{3.10}$$

with

$$\lambda_\perp = \tfrac{1}{4}\zeta^* - \eta^* k^2, \tag{3.11}$$

and the threshold for this shear mode is given by

$$k_\perp = \frac{1}{2}\sqrt{\frac{\zeta^*}{\eta^*}}. \tag{3.12}$$

From (3.6*a*), (3.6*b*) and (3.6*d*), the other three eigenmodes λ_i $(i = 1, 2, 3)$ can be obtained as the solutions of the third-order equation

$$\begin{aligned} &\lambda^3 + \left[\left(A - \frac{1}{4}\right)\zeta^* + \left(\frac{4}{3}\eta^* + \frac{5}{2}\kappa^*\right)k^2\right]\lambda^2 \\ &\quad + \left[-\frac{1}{4}A\zeta^{*2} + \left(\frac{5}{6} + \frac{4}{3}A\zeta^*\eta^* - \frac{5}{8}\zeta^*\kappa^*\right)k^2 + \frac{10}{3}\eta^*\kappa^* k^4\right]\lambda \\ &\quad + \left[\left(\frac{A}{2} - \frac{1}{4}\right)\zeta^* k^2 + \frac{5}{4}(\kappa^* - \mu^*)k^4\right] = 0. \end{aligned} \tag{3.13}$$

We can numerically obtain the thresholds for the heat mode and the sound modes from (3.13).

Figure 6 shows the wavenumber dependence of each mode. In the regime of high granular temperature, the real part of the heat mode becomes positive for small k, rendering the heat mode unstable. In contrast, the sound mode is unstable for all k. For $T \simeq 1.6T^*$ and large k, the real parts of the heat mode are almost equal to those of the sound modes. For a smaller granular temperature, the real part of the heat mode is negative for all k and the real parts of the sound modes become positive for small k, which is not observed for hard-sphere gases. Figure 7 shows the granular temperature dependencies of the threshold values for the shear mode, the heat mode and the sound mode, where k_h and k_s are the wavenumbers where (3.13) is satisfied. In the limit of high granular temperature, both thresholds correspond to elastic or dissipative hard-sphere gases. On the other hand, the

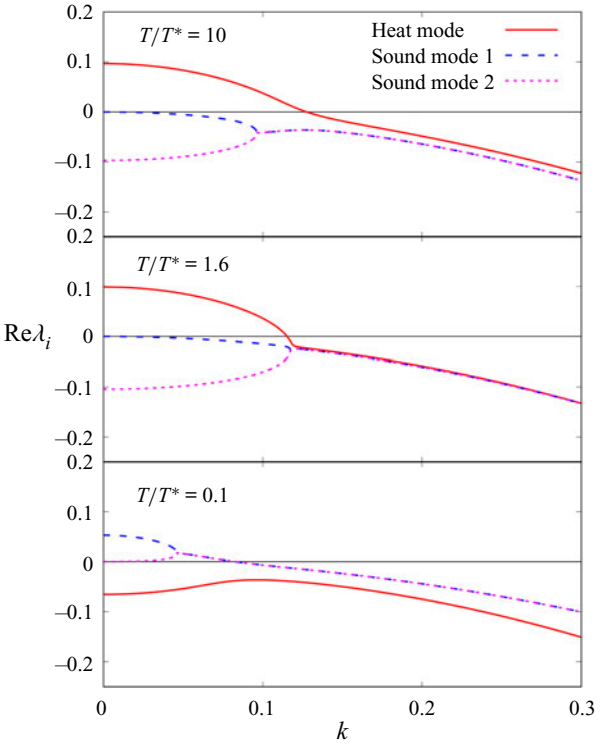

Figure 6. The wavenumber dependence of the real parts of the heat mode (solid line) and the sound mode (dashed and dotted lines) for $T/T^* = 10$, 1.6, and 0.1 and $e^* = 0.8$.

threshold for the heat mode becomes imaginary below $0.5T^*$, while that for the shear mode decreases to zero. Below $1.6T^*$, as shown in figure 6, the real part of the heat mode becomes negative while those of the sound modes become positive for small k. In addition, the threshold for the sound modes has a peak around $0.3T^*$.

We wish to mention that in the limit $x \to 0$, we obtain $A \to \frac{1}{4}$ and the structure of (3.11) and (3.13) is consistent with previous results obtained by Garzó (2005) for hard spheres.

4. Numerical confirmation of the results

In order to validate the theoretical results presented in the preceding sections, we performed event-driven molecular dynamics simulations of the granular system. In particular, here we focus on the numerical measurement of the shear viscosity. Obviously, the shear viscosity in a system operating in the homogeneous cooling state is different from the shear viscosity in a uniformly sheared phase (Santos, Garzó & Dufty 2004; Takada *et al.* 2016; Takada & Hayakawa 2018). Consequently, we must not determine numerically the value of shear viscosity in the traditional way. Instead, for systems in the homogeneous cooling state, Brey & Cubero (2001) introduced a protocol to determine the shear viscosity from a relaxation process, that is, a perturbation is added to the system and the relaxation is observed.

We consider a set of $N = 3000$ particles of mass m and diameter σ homogeneously distributed in a cubic box of side length $L = 54\,\sigma$ with periodic boundary conditions. The given parameters correspond to a packing fraction of $\phi = 1.0 \times 10^{-2}$ (corresponding to

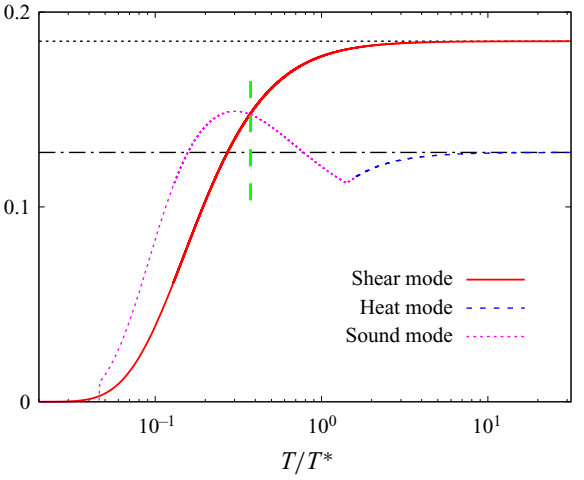

Figure 7. Threshold values of the shear mode (solid line), the heat mode (dashed line) and the sound modes (dotted line) as functions of the granular temperature for $e^* = 0.8$. The dotted black line shows the value of the shear mode for a hard-sphere gas. The dot-dashed line refers to the heat mode of a hard-sphere gas. The dashed green line highlights the value $T/T^* \approx 0.4$ where the threshold for the heat mode turns imaginary.

the number density $n\sigma^3 \simeq 1.9 \times 10^{-2}$). We add a velocity perturbation via

$$u_y(x, t = 0) \propto \sin\left(\frac{2\pi}{L}x\right) \tag{4.1}$$

and observe the relaxation back to the uniform state in the course of time. Following Brey & Cubero (2001) and using (3.3*a–c*) and (3.10), the value of the shear viscosity, η^*, can be obtained from

$$u_y(x, t) \propto \exp(-\eta^* k^2 \tau). \tag{4.2}$$

Figure 3 (black square symbols) shows the shear viscosity determined by means of (4.2) in comparison with the theoretical results. In the whole range of the granular temperature, the result is consistent with the theory (2.27). Small deviations of the molecular dynamics simulation data from the theory arise due to the statistical nature of the particle system (Brey & Cubero 2001).

Note that an molecular dynamics numerical confirmation of the thermal conductivity and the Dufour-like coefficient μ in a granular system is much more complicated since these two coefficients are coupled (Dufty & Brey 2002; Brey & Ruiz-Montero 2004; Brey *et al.* 2005).

5. Discussion

To check the validity of the perturbative solution of (2.25*a*,*b*) to derive the shear viscosity, we relate the first terms of (2.27) and obtain

$$\begin{aligned}\frac{\eta^{*(1)}}{\eta^{*(0)}} &= \frac{10x\mu_2}{5\mu_2 + 6\Omega_\eta^e}\frac{\partial}{\partial x}\log\eta^{*(0)} \\ &= -\frac{10x\mu_2}{(5\mu_2 + 6\Omega_\eta^e)^2}\left(5\frac{\partial\mu_2}{\partial x} + 6\frac{\partial\Omega_\eta^e}{\partial x}\right).\end{aligned} \tag{5.1}$$

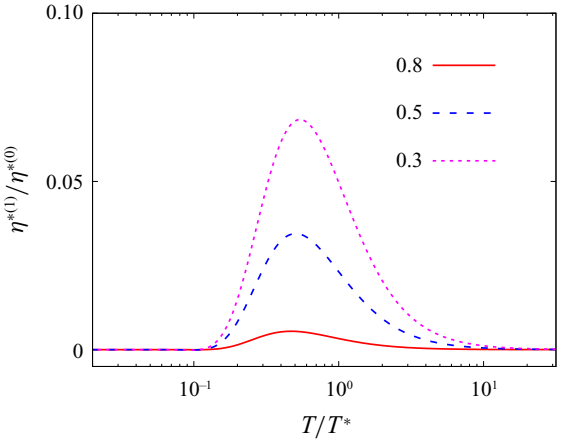

Figure 8. The ratio $\eta^{*(1)}$ to $\eta^{*(0)}$ of the first terms of (2.27) as a function of granular temperature for the restitution coefficient $e^* = 0.8$ (solid line), $e^* = 0.5$ (dashed line) and $e^* = 0.3$ (dotted line).

Figure 8 shows this ratio as a function of the granular temperature for various values of the coefficient of restitution, e^*. Even for moderately large inelasticity, we obtain $\eta^{*(1)}/\eta^{*(0)} \ll 1$, justifying the perturbation solution.

Let us analyse the crossover behaviour of the viscosity. We define the effective restitution coefficient e_{eff} (Takada *et al.* 2017) as

$$1 - e_{eff}^2 = (1 - e^{*2})(1 + x)e^{-x}, \tag{5.2}$$

where the right-hand side of (5.2) is equivalent to S_1 for $\beta v^* \to \infty$ given by (A10*a*). The hard-sphere limit of a_2 with this effective restitution coefficient is known to reproduce the peak value of a_2 in figure 1 (Takada *et al.* 2017). Let us define the effective shear viscosity as

$$\eta_{eff} = \frac{15}{2(1 + e_{eff})(13 - e_{eff})\sigma^2}\sqrt{\frac{mT}{\pi}}\left[1 + \frac{3(4 - 3e_{eff})}{8(13 - e_{eff})}a_{2,eff} + \frac{(7 - 4e_{eff})}{32(13 - e_{eff})}a_{3,eff}\right], \tag{5.3}$$

with $a_{2,eff} \equiv a_2^{(HC)}(e_{eff})$ and $a_{3,eff} \equiv a_3^{(HC)}(e_{eff})$. Figure 9 represents the granular temperature dependence of the effective shear viscosity (5.3). This simple effective theory (5.2) well reproduces the crossover granular temperature between two regimes.

We also consider the reason for the negativity of the coefficient μ in the intermediate granular temperature regime. Upon considering the relaxation dynamics of the hydrodynamic fluxes by mean of a Grad expansion pertaining to granular gases, it was shown by Sela & Goldhirsch (1998), Serero *et al.* (2009) and Serero (2009) that the origin of the contribution to the heat flux proportional to the gradient of the density could be traced back to the time dependence in granular gases of the microscopic time scale (the means free time). In the case of the heat flux, this dependence manifests itself through the emergence in the post-relaxation expression of the heat flux of a gradient of the cooling coefficient (Serero *et al.* 2009; Serero 2009) (expressing the difference in the dynamics of the granular temperature on the sub-resolved scale), giving rise to a gradient of the density (see Serero (2009) and Serero *et al.* (2009) for a detailed derivation in the case of a monodisperse and bidisperse system of inelastic hard spheres, respectively). In the present case, this mechanism can yield a negative μ coefficient when combined with

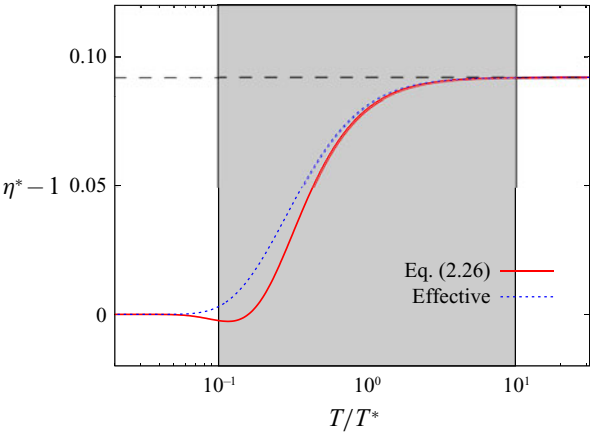

Figure 9. The granular temperature dependence of the shear viscosity obtained from the kinetic theory up to a_3 order (solid line) and that from the effective theory (dotted line). The dashed line is the shear viscosity of hard-sphere gases $\eta^{(HC)}(e^*)$. The crossover regime ($10^{-1} \lesssim T/T^* \lesssim 10^{1}$) is highlighted in grey.

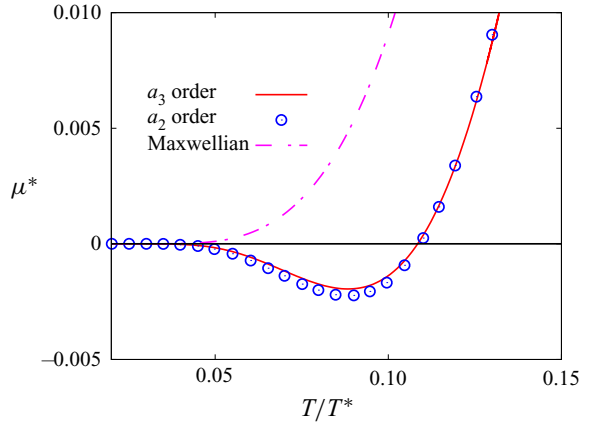

Figure 10. The granular temperature dependence of the coefficient μ obtained from the kinetic theory up to a_3 order (solid line), that up to a_2 order (open circles) and that determined from the Maxwell distribution function (dot-dashed line) for $e^* = 0.8$.

the particular form of the distribution function at hand, as detailed below. Note that this cannot be observed when we only use the Maxwell distribution function to determine the coefficient μ as shown in figure 10, which means that the origin of the negativeness comes from the deviation of the distribution function from the Gaussian. Let us consider two regions, one of which is slightly denser (system I) and the other is diluter (system II) with the same granular temperature around $T/T^* \simeq 0.1$. Although the distribution function is the same, the number of particles is different. Because the number of particles whose velocity is higher than v^* in system I is larger, the number of inelastic collisions increases, and the granular temperature of the former decays slightly faster than that of the latter. As a result, the granular temperature in system I is slightly smaller than that in system II ($T_I \lesssim T_{II}$), and this yields $a_2(T_I) \gtrsim a_2(T_{II})$. In addition, as our previous paper (Takada *et al.* 2017) reported, the population of the particles having $1 \lesssim v/v_T \lesssim 2$ and $v/v_T \gtrsim 2$ in system I are higher and lower than those in system II, respectively (in this case, $v_T \simeq 0.3v^*$). Therefore, the heat flux goes from system II to system I, because the

number of particles having higher velocities is larger in system II. This is the reason for the negative overshoot of μ in the intermediate granular temperature regime. It is noted that the transient behaviour of the thermal conductivity is similarly explained. Note that the effect of a negative coefficient μ was also reported for driven granular gases by González & Garzó (2019) and for confined quasi-two-dimensional granular gases by Brey *et al.* (2015) and Garzó, Brito & Soto (2018).

6. Conclusion

In this paper we have derived the granular temperature dependence of the transport coefficients for charged granular gases in the discontinuous limit of the effective restitution coefficient. The negative overshoots of the transport coefficients appear because of the non-Gaussianity of the distribution function. Especially, we have found that the coefficient μ becomes negative in the intermediate granular temperature regime. We have also performed the linear stability analysis for the homogeneous cooling state, which shows that the stability of the thermal and sound modes become reversal in the low granular temperature regime, and this threshold is about $0.5T^*$. We have also performed the molecular dynamics simulation and we have obtained a consistent result with that from the kinetic theory.

Acknowledgements. S.T. wishes to express his sincere gratitude to the Yukawa Institute for Theoretical Physics for financial support towards his research visit at Friedrich-Alexander-Universität Erlangen-Nürnberg. Numerical computation in this work was partially carried out at the Yukawa Institute Computer Facility. We thank the Interdisciplinary Center for Nanostructured Films (IZNF), the Central Institute for Scientific Computing (ZISC) and the Interdisciplinary Center for Functional Particle Systems (FPS) at Friedrich-Alexander University Erlangen-Nürnberg.

Funding. This work was supported by Kompetenznetzwerk für wissenschaftliches Höchstleistungsrechnen in Bayern (KONWIHR) Satoshi Takada is partially supported by Scientific Grant-in-Aid of Japan Society for the Promotion of Science, KAKENHI (grants nos. 20K14428 and 21H01006).

Declaration of interests. The authors report no conflict of interest.

Author ORCIDs.
Satoshi Takada https://orcid.org/0000-0002-2716-1846;
Thorsten Pöschel https://orcid.org/0000-0001-5913-1070.

Appendix A. Computation of the Sonine coefficients a_2 and a_3 from the Boltzmann equation

We expand the distribution function in Sonine polynomials up to third order, a_3; see (2.4). Then, we rewrite the expression of the pth moment of the collision integral in the form

$$\mu_p = -\frac{1}{2}\int \mathrm{d}\boldsymbol{C}\,\mathrm{d}\boldsymbol{c}_{12}\,\mathrm{d}\hat{\boldsymbol{k}}\,\Theta(\boldsymbol{c}_{12}\cdot\hat{\boldsymbol{k}})\left|\boldsymbol{c}_{12}\cdot\hat{\boldsymbol{k}}\right|\phi(c_1)\phi(c_2)$$
$$\times\left\{1+a_2\left[S_2(c_1^2)+S_2(c_2^2)\right]+a_3\left[S_3(c_1^2)+S_3(c_2^2)\right]\right\}\Delta(c_1^p+c_2^p), \tag{A1}$$

where we have neglected the terms proportional to a_2^2, a_3^2 and a_2a_3. The product of the dimensionless distribution function is then

$$1+a_2\left[S_2(c_1^2)+S_2(c_2^2)\right]+a_3\left[S_3(c_1^2)+S_3(c_2^2)\right]$$
$$=1+a_2\left[C^4+\tfrac{1}{2}C^2c_{12}^2-5C^2+\tfrac{1}{16}c_{12}^4-\tfrac{5}{4}c_{12}^2+(\boldsymbol{C}\cdot\boldsymbol{c}_{12})^2+\tfrac{15}{4}\right]$$

$$+a_3\left[-\tfrac{1}{3}C^6-\tfrac{1}{4}C^4c_{12}^2+\tfrac{7}{2}C^4-\tfrac{1}{16}C^2c_{12}^4+\tfrac{7}{4}C^2c_{12}^2-C^2(\boldsymbol{C}\cdot\boldsymbol{c}_{12})^2-\tfrac{35}{4}C^2\right.$$
$$\left.-\tfrac{1}{192}c_{12}^6+\tfrac{7}{32}c_{12}^4-\tfrac{1}{4}c_{12}^2(\boldsymbol{C}\cdot\boldsymbol{c}_{12})^2-\tfrac{35}{16}c_{12}^2+\tfrac{7}{2}(\boldsymbol{C}\cdot\boldsymbol{c}_{12})^2+\tfrac{35}{8}\right], \tag{A2}$$

and the terms $\Delta(c_1^p+c_2^p)$ for $p=2$, 4 and 6 are, respectively, given by

$$\Delta(c_1^2+c_2^2)=-\frac{1-e^2}{2}(\boldsymbol{c}_{12}\cdot\hat{\boldsymbol{k}})^2, \tag{A3a}$$

$$\begin{aligned}\Delta(c_1^4+c_2^4)=&-(1-e^2)C^2(\boldsymbol{c}_{12}\cdot\hat{\boldsymbol{k}})^2-\frac{1}{4}(1-e^2)c_{12}^2(\boldsymbol{c}_{12}\cdot\hat{\boldsymbol{k}})^2\\&-4(1+e)(\boldsymbol{C}\cdot\boldsymbol{c}_{12})(\boldsymbol{C}\cdot\hat{\boldsymbol{k}})(\boldsymbol{c}_{12}\cdot\hat{\boldsymbol{k}})\\&+2(1+e)^2(\boldsymbol{C}\cdot\hat{\boldsymbol{k}})^2(\boldsymbol{c}_{12}\cdot\hat{\boldsymbol{k}})^2+\frac{(1-e^2)^2}{8}(\boldsymbol{c}_{12}\cdot\hat{\boldsymbol{k}})^4,\end{aligned} \tag{A3b}$$

$$\begin{aligned}\Delta(c_1^6+c_2^6)=&-\frac{3(1-e^2)}{2}C^4(\boldsymbol{c}_{12}\cdot\hat{\boldsymbol{k}})^2-\frac{3(1-e^2)}{4}C^2c_{12}^2(\boldsymbol{c}_{12}\cdot\hat{\boldsymbol{k}})^2\\&-12(1+e)C^2(\boldsymbol{C}\cdot\boldsymbol{c}_{12})(\boldsymbol{C}\cdot\hat{\boldsymbol{k}})(\boldsymbol{c}_{12}\cdot\hat{\boldsymbol{k}})+6(1+e)^2C^2(\boldsymbol{C}\cdot\hat{\boldsymbol{k}})^2(\boldsymbol{c}_{12}\cdot\hat{\boldsymbol{k}})^2\\&+\frac{3(1-e^2)^2}{8}C^2(\boldsymbol{c}_{12}\cdot\hat{\boldsymbol{k}})^4-\frac{3(1-e^2)}{32}c_{12}^4(\boldsymbol{c}_{12}\cdot\hat{\boldsymbol{k}})^2\\&-3(1+e)c_{12}^2(\boldsymbol{C}\cdot\boldsymbol{c}_{12})(\boldsymbol{C}\cdot\hat{\boldsymbol{k}})(\boldsymbol{c}_{12}\cdot\hat{\boldsymbol{k}})+\frac{3(1+e)^2}{2}c_{12}^2(\boldsymbol{C}\cdot\hat{\boldsymbol{k}})^2(\boldsymbol{c}_{12}\cdot\hat{\boldsymbol{k}})^2\\&+\frac{3(1-e^2)^2}{32}c_{12}^2(\boldsymbol{c}_{12}\cdot\hat{\boldsymbol{k}})^4-\frac{3(1-e^2)}{2}(\boldsymbol{C}\cdot\boldsymbol{c}_{12})^2(\boldsymbol{c}_{12}\cdot\hat{\boldsymbol{k}})^2\\&+3(1+e)(1-e^2)(\boldsymbol{C}\cdot\boldsymbol{c}_{12})(\boldsymbol{C}\cdot\hat{\boldsymbol{k}})(\boldsymbol{c}_{12}\cdot\hat{\boldsymbol{k}})^3\\&-\frac{3(1+e)^2(1-e^2)}{2}(\boldsymbol{C}\cdot\hat{\boldsymbol{k}})^2(\boldsymbol{c}_{12}\cdot\hat{\boldsymbol{k}})^4-\frac{(1-e^2)^3}{32}(\boldsymbol{c}_{12}\cdot\hat{\boldsymbol{k}})^6.\end{aligned} \tag{A3c}$$

Using (A2)–(A3c), we can calculate μ_p for $p=2$, 4 and 6 from (A1) as

$$\mu_2=\sqrt{2\pi}(S_1+a_2S_2+a_3S_3), \tag{A4a}$$
$$\mu_4=\sqrt{2\pi}(T_1+a_2T_2+a_3T_3), \tag{A4b}$$
$$\mu_6=\sqrt{2\pi}(D_1+a_2D_2+a_3D_3), \tag{A4c}$$

with

$$S_1=\tfrac{1}{2}\int_0^\infty \mathrm{d}c_{12}\int_0^1 \mathrm{d}(\cos\theta)(1-e^2)\cos^3\theta c_{12}^5\exp\left(-\tfrac{1}{2}c_{12}^2\right), \tag{A5a}$$

$$S_2=\tfrac{1}{32}\int_0^\infty \mathrm{d}c_{12}\int_0^1 \mathrm{d}(\cos\theta)(1-e^2)\cos^3\theta c_{12}^5(15-10c_{12}^2+c_{12}^4)\exp\left(-\tfrac{1}{2}c_{12}^2\right), \tag{A5b}$$

$$S_3 = \tfrac{1}{384}\int_0^\infty \mathrm{d}c_{12}\int_0^1 \mathrm{d}(\cos\theta)(1-e^2)\cos^3\theta c_{12}^5 \times (105 - 105c_{12}^2 + 21c_{12}^4 - c_{12}^6)\exp\left(-\tfrac{1}{2}c_{12}^2\right), \tag{A5c}$$

$$T_1 = \tfrac{1}{8}\int_0^\infty \mathrm{d}c_{12}\int_0^1 \mathrm{d}(\cos\theta)(1-e^2)\cos^3\theta c_{12}^5 \times \left[10 + 2c_{12}^2 - (1-e^2)\cos^2\theta c_{12}^2\right]\exp\left(-\tfrac{1}{2}c_{12}^2\right), \tag{A6a}$$

$$\begin{aligned} T_2 = {} & \tfrac{1}{2}\int_0^\infty \mathrm{d}c_{12}\int_0^1 \mathrm{d}(\cos\theta)(1+e)\cos^3\theta c_{12}^5\exp\left(-\tfrac{1}{2}c_{12}^2\right) \\ & + \tfrac{1}{128}\int_0^\infty \mathrm{d}c_{12}\int_0^1 \mathrm{d}(\cos\theta)(1-e^2)\cos^3\theta c_{12}^5\exp\left(-\tfrac{1}{2}c_{12}^2\right) \\ & \times \left[2(-25 - 7c_{12}^2 - 5c_{12}^4 + c_{12}^6) + \cos^2\theta c_{12}^2(17 + 10c_{12}^2 - c_{12}^4)\right. \\ & \left. + e^2\cos^2\theta c_{12}^2(15 - 10c_{12}^2 + c_{12}^4)\right], \end{aligned} \tag{A6b}$$

$$\begin{aligned} T_3 = {} & \tfrac{1}{8}\int_0^\infty \mathrm{d}c_{12}\int_0^1 \mathrm{d}(\cos\theta)(1+e)\cos^3\theta(1-\cos^2\theta)c_{12}^7(7-c_{12}^2)\exp\left(-\tfrac{1}{2}c_{12}^2\right) \\ & + \tfrac{1}{1536}\int_0^\infty \mathrm{d}c_{12}\int_0^1 \mathrm{d}(\cos\theta)(1-e^2)\cos^3\theta c_{12}^5\exp\left(-\tfrac{1}{2}c_{12}^2\right) \\ & \times \left[2(-525 + 168c_{12}^2 - 54c_{12}^4 + 16c_{12}^6 - c_{12}^8) + \cos^2\theta c_{12}^2(567 + 9c_{12}^2 - 21c_{12}^4 + c_{12}^6)\right. \\ & \left. + e^2\cos^2\theta c_{12}^2(105 - 105c_{12}^2 + 21c_{12}^4 - c_{12}^6)\right], \end{aligned} \tag{A6c}$$

$$D_1 = \tfrac{1}{32}\int_0^\infty \mathrm{d}c_{12}\int_0^1 \mathrm{d}(\cos\theta)(1-e^2)\cos^3\theta c_{12}^5\exp\left(-\tfrac{1}{2}c_{12}^2\right) \times \left[3(35 + 14c_{12}^2 + c_{12}^4) - 3(1-e^2)\cos^2\theta c_{12}^2(7 + c_{12}^2) + (1-e^2)^2\cos^4\theta c_{12}^4\right], \tag{A7a}$$

$$\begin{aligned} D_2 = {} & \tfrac{3}{16}\int_0^\infty \mathrm{d}c_{12}\int_0^1 \mathrm{d}(\cos\theta)(1+e)\cos^3\theta c_{12}^7 \\ & \times \left[2 - (1+e)\cos^2\theta\right]\left[7 + c_{12}^2 - (1-e^2)\cos^2\theta c_{12}^2\right]\exp\left(-\tfrac{1}{2}c_{12}^2\right) \\ & + \tfrac{1}{512}\int_0^\infty \mathrm{d}c_{12}\int_0^1 \mathrm{d}(\cos\theta)(1-e^2)\cos^3\theta c_{12}^5\exp\left(-\tfrac{1}{2}c_{12}^2\right) \\ & \times \left[3(-595 - 28c_{12}^2 + 14c_{12}^4 + 4c_{12}^6 + c_{12}^8)\right. \\ & + 3(1-e^2)\cos^2\theta c_{12}^2(35 + 19c_{12}^2 + 3c_{12}^4 - c_{12}^6) \\ & \left. + (1-e^2)^2\cos^4\theta c_{12}^4(15 - 10c_{12}^2 + c_{12}^4)\right], \end{aligned} \tag{A7b}$$

$$D_3 = \tfrac{3}{64}\int_0^\infty \mathrm{d}c_{12}\int_0^1 \mathrm{d}(\cos\theta)(1+e)\cos^3\theta c_{12}^7\exp\left(-\tfrac{1}{2}c_{12}^2\right) \times \left[2 - (1+e)\cos^2\theta\right]\left[35 - c_{12}^4 - (1-e^2)\cos^2\theta c_{12}^2(7 - c_{12}^2)\right]$$

$$+\tfrac{1}{6144}\int_0^\infty \mathrm{d}c_{12}\int_0^1 \mathrm{d}(\cos\theta)(1-e^2)\cos^3\theta c_{12}^5\exp\left(-\tfrac{1}{2}c_{12}^2\right)$$
$$\times\left[3(-5145+1575c_{12}^2+798c_{12}^4-74c_{12}^6+7c_{12}^8-c_{12}^{10})\right.$$
$$+3(1-e^2)\cos^2\theta c_{12}^2(735-126c_{12}^2+24c_{12}^4-14c_{12}^6+c_{12}^8)$$
$$\left.+(1-e^2)^2\cos^4\theta c_{12}^4(105-105c_{12}^2+21c_{12}^4-c_{12}^6)\right]. \tag{A7c}$$

Here, we use the relations between the moments μ_p of different order,

$$\mu_4 = 5\mu_2(1+2a_2), \tag{A8a}$$
$$\mu_6 = \tfrac{105}{4}\mu_2(1+3a_2-a_3). \tag{A8b}$$

Substituting (A4) into (A8), we obtain

$$(5S_1+5S_2-T_2)a_2+(5S_3-T_3)a_3 = T_1-5S_1, \tag{A9a}$$
$$\left(\tfrac{315}{4}S_1+\tfrac{105}{4}S_2-D_2\right)a_2+\left(-\tfrac{105}{4}S_1+\tfrac{105}{4}S_3-D_3\right)a_3 = D_1-\tfrac{105}{4}S_1. \tag{A9b}$$

Using (A9), we obtain the coefficients a_2 and a_3 in the form given by (2.9a,b).

In the discontinuous limit, $\beta v^* \to \infty$, (A5a)–(A7c) read as

$$S_1^{(\infty)}(x) = \left(1-e^{*2}\right)(1+x)e^{-x}, \tag{A10a}$$
$$S_2^{(\infty)}(x) = \frac{3}{16}\left(1-e^{*2}\right)\left(1+x+\frac{x^2}{3}\right)e^{-x}, \tag{A10b}$$
$$S_3^{(\infty)}(x) = \tfrac{1}{64}\left(1-e^{*2}\right)\left(1+x-2x^2+\tfrac{28}{3}x^3-\tfrac{8}{3}x^4\right)e^{-x}, \tag{A10c}$$

$$T_1^{(\infty)}(x) = \left(1-e^{*2}\right)\left[\frac{9}{2}\left(1+x+\frac{x^2}{9}\right)+e^{*2}\left(1+x+\frac{x^2}{2}\right)\right]e^{-x}, \tag{A11a}$$
$$T_2^{(\infty)}(x) = \frac{3}{32}\left(1-e^{*2}\right)\left[69\left(1+x+\frac{119x^2}{207}+\frac{32x^3}{207}+\frac{4x^4}{207}\right)\right.$$
$$\left.+10e^{*2}\left(1+x+\frac{x^2}{2}+\frac{2x^3}{15}+\frac{2x^4}{15}\right)\right]e^{-x}$$
$$-2\left(1-e^{*}\right)(1+x)e^{-x}+4, \tag{A11b}$$
$$T_3^{(\infty)}(x) = -\frac{1}{128}(1-e^{*2})\left[117\left(1+x+\frac{19}{117}x^2+\frac{10}{13}x^3+\frac{4}{39}x^4+\frac{8}{351}x^5\right)\right.$$
$$\left.+10e^{*2}\left(1+x+\frac{x^2}{2}+\frac{x^3}{3}-\frac{2x^4}{3}+\frac{4x^5}{15}\right)\right]e^{-x}$$
$$+\frac{1}{2}(1-e^{*})(1+x+2x^2)e^{-x}-1, \tag{A11c}$$

$$D_1^{(\infty)}(x) = \frac{3}{16}(1-e^{*2})\left[115\left(1+x+\frac{22x^2}{115}+\frac{4x^3}{345}\right)+44e^{*2}\left(1+x+\frac{x^2}{2}+\frac{x^3}{33}\right)\right.$$
$$\left.+8e^{*4}\left(1+x+\frac{x^2}{2}+\frac{x^3}{6}\right)\right]e^{-x}, \tag{A12a}$$

$$D_2^{(\infty)}(x) = \frac{3}{256}(1-e^{*2})\left[5737\left(1+x+\frac{2850x^2}{5737}+\frac{2120x^3}{17\,211}+\frac{248x^4}{17\,211}+\frac{16x^5}{17\,211}\right)\right.$$
$$+1572e^{*2}\left(1+x+\frac{x^2}{2}+\frac{221x^3}{1179}+\frac{62x^4}{1179}+\frac{4x^5}{1179}\right)$$
$$\left.+280e^{*4}\left(1+x+\frac{x^2}{2}+\frac{x^3}{6}+\frac{4x^4}{105}+\frac{2x^5}{105}\right)\right]e^{-x}$$
$$+\frac{3}{2}(1+e^*)\left[20\left(1+x+\frac{9x^2}{40}\right)-9e^*\left(1+x+\frac{x^2}{2}\right)\right.$$
$$\left.+10e^{*2}\left(1+x+\frac{x^2}{2}+\frac{x^3}{10}\right)-6e^{*3}\left(1+x+\frac{x^2}{2}+\frac{x^3}{6}\right)\right]e^{-x}$$
$$-45\left(1+x+\frac{2x^2}{15}\right)e^{-x}+45, \tag{A12b}$$

$$D_3^{(\infty)}(x) = -\frac{3}{1024}(1-e^{*2})\left[9161\left(1+x+\frac{4528x^2}{9161}+\frac{2132x^3}{9161}+\frac{1640x^4}{27\,483}\right.\right.$$
$$\left.+\frac{128x^5}{27\,483}+\frac{32x^6}{27\,483}\right)$$
$$+1636e^{*2}\left(1+x+\frac{x^2}{2}+\frac{140x^3}{1227}+\frac{76x^4}{1227}+\frac{32x^5}{1227}+\frac{8x^6}{3681}\right)$$
$$\left.+280e^{*4}\left(1+x+\frac{x^2}{2}+\frac{x^3}{6}+\frac{x^4}{21}-\frac{2x^5}{105}+\frac{4x^6}{315}\right)\right]e^{-x}$$
$$-\frac{9}{8}(1+e^*)\left[20\left(1+x+\frac{71x^2}{120}+\frac{3x^3}{20}\right)-9e^*\left(1+x+\frac{x^2}{2}+\frac{x^3}{3}\right)\right.$$
$$+10e^{*2}\left(1+x+\frac{x^2}{2}+\frac{7x^3}{30}+\frac{x^4}{15}\right)$$
$$\left.-6e^{*3}\left(1+x+\frac{x^2}{2}+\frac{x^3}{6}+\frac{x^4}{9}\right)\right]e^{-x}$$
$$+\frac{135}{4}\left(1+x+\frac{28x^2}{45}+\frac{4x^3}{45}\right)e^{-x}-\frac{135}{4}. \tag{A12c}$$

It can be shown that in the limit $x \to 0$, the above expressions are identical to the corresponding expressions for a hard-sphere gas (Brilliantov & Pöschel 2006; Santos & Montanero 2009; Chamorro *et al.* 2013). Using (A9), we can also obtain explicit expressions for a_2 and a_3. These expressions are rather cumbersome and not shown here.

Appendix B. Calculation of Ω^e_η and Ω^e_κ given by (2.11) and (2.14)

Using the definition of $\tilde{D}_{\alpha\beta}(\boldsymbol{c})$, (2.12), we obtain

$$\begin{aligned}
&\tilde{D}_{\alpha\beta}(\boldsymbol{c}_2)\Delta[\tilde{D}_{\alpha\beta}(\boldsymbol{c}_1)+\tilde{D}_{\alpha\beta}(\boldsymbol{c}_2)]\\
&\quad=\left(c_{2i}c_{2j}-\frac{1}{3}\delta_{ij}c_2^2\right)\left[c'_{1i}c'_{1j}+c'_{2i}c'_{2j}-c_{1i}c_{1j}-c_{2i}c_{2j}-\frac{1}{3}\delta_{ij}\left(c_1'^2+c_2'^2-c_1^2-c_2^2\right)\right]\\
&\quad=\frac{1-e^2}{6}C^2(\boldsymbol{c}_{12}\cdot\hat{\boldsymbol{k}})^2+\frac{1+e}{2}c_{12}^2(\boldsymbol{C}\cdot\hat{\boldsymbol{k}})(\boldsymbol{c}_{12}\cdot\hat{\boldsymbol{k}})-\frac{(1+e)(5+e)}{24}c_{12}^2(\boldsymbol{c}_{12}\cdot\hat{\boldsymbol{k}})^2\\
&\qquad-(1+e)(\boldsymbol{C}\cdot\boldsymbol{c}_{12})(\boldsymbol{C}\cdot\hat{\boldsymbol{k}})(\boldsymbol{c}_{12}\cdot\hat{\boldsymbol{k}})+\frac{(1+e)(2+e)}{6}(\boldsymbol{C}\cdot\boldsymbol{c}_{12})(\boldsymbol{c}_{12}\cdot\hat{\boldsymbol{k}})^2\\
&\qquad+\frac{(1+e)^2}{2}(\boldsymbol{C}\cdot\hat{\boldsymbol{k}})^2(\boldsymbol{c}_{12}\cdot\hat{\boldsymbol{k}})^2-\frac{(1+e)^2}{2}(\boldsymbol{C}\cdot\hat{\boldsymbol{k}})(\boldsymbol{c}_{12}\cdot\hat{\boldsymbol{k}})^3+\frac{(1+e)^2}{8}(\boldsymbol{c}_{12}\cdot\hat{\boldsymbol{k}})^4.
\end{aligned}\tag{B1}$$

We also use the expressions of the Sonine expansion as

$$\begin{aligned}
&1+a_2S_2(c_1)^2+a_3S_3(c_1^2)\\
&\quad=1+a_2\left[\tfrac{1}{2}C^4+\tfrac{1}{4}C^2c_{12}^2+C^2(\boldsymbol{C}\cdot\boldsymbol{c}_{12})-\tfrac{5}{2}C^2+\tfrac{1}{32}c_{12}^4\right.\\
&\qquad\left.+\tfrac{1}{4}c_{12}^2(\boldsymbol{C}\cdot\boldsymbol{c}_{12})-\tfrac{5}{8}c_{12}^2+\tfrac{1}{2}(\boldsymbol{C}\cdot\boldsymbol{c}_{12})^2-\tfrac{5}{2}(\boldsymbol{C}\cdot\boldsymbol{c}_{12})+\tfrac{15}{8}\right]\\
&\qquad+a_3\left[-\tfrac{1}{6}C^6-\tfrac{1}{8}C^4c_{12}^2-\tfrac{1}{2}C^4(\boldsymbol{C}\cdot\boldsymbol{c}_{12})+\tfrac{7}{4}C^4-\tfrac{1}{32}C^2c_{12}^4-\tfrac{1}{4}C^2c_{12}^2(\boldsymbol{C}\cdot\boldsymbol{c}_{12})\right.\\
&\qquad+\tfrac{7}{8}C^2c_{12}^2-\tfrac{1}{2}C^2(\boldsymbol{C}\cdot\boldsymbol{c}_{12})^2+\tfrac{7}{2}C^2(\boldsymbol{C}\cdot\boldsymbol{c}_{12})-\tfrac{35}{8}C^2-\tfrac{1}{384}c_{12}^6\\
&\qquad-\tfrac{1}{32}c_{12}^4(\boldsymbol{C}\cdot\boldsymbol{c}_{12})+\tfrac{7}{64}c_{12}^4-\tfrac{1}{8}c_{12}^2(\boldsymbol{C}\cdot\boldsymbol{c}_{12})^2+\tfrac{7}{8}c_{12}^2(\boldsymbol{C}\cdot\boldsymbol{c}_{12})\\
&\qquad\left.-\tfrac{35}{32}c_{12}^2-\tfrac{1}{6}(\boldsymbol{C}\cdot\boldsymbol{c}_{12})^3+\tfrac{7}{4}(\boldsymbol{C}\cdot\boldsymbol{c}_{12})^2-\tfrac{35}{8}(\boldsymbol{C}\cdot\boldsymbol{c}_{12})+\tfrac{35}{16}\right].
\end{aligned}\tag{B2}$$

Substituting (B1) and (B2) into (2.11), we obtain

$$\Omega^e_\eta\equiv\sqrt{2\pi}\left(\omega^e_{\eta,1}+a_2\omega^e_{\eta,2}+a_3\omega^e_{\eta,3}\right),\tag{B3}$$

with

$$\begin{aligned}
\omega^e_{\eta,1}&=-\tfrac{1}{12}\int_0^\infty \mathrm{d}c_{12}\int_0^1\mathrm{d}(\cos\theta)(1+e)\left[5+e-3(1+e)\cos^2\theta\right]\\
&\qquad\times\cos^3\theta c_{12}^7\exp\left(-\tfrac{1}{2}c_{12}^2\right),
\end{aligned}\tag{B4a}$$

$$\begin{aligned}
\omega^e_{\eta,2}&=-\tfrac{1}{384}\int_0^\infty \mathrm{d}c_{12}\int_0^1\mathrm{d}(\cos\theta)(1+e)\left[5+e-3(1+e)\cos^2\theta\right]\\
&\qquad\times\cos^3\theta c_{12}^7(63-18c_{12}^2+c_{12}^4)\exp\left(-\tfrac{1}{2}c_{12}^2\right),
\end{aligned}\tag{B4b}$$

$$\begin{aligned}
\omega^e_{\eta,3}&=-\tfrac{1}{4608}\int_0^\infty \mathrm{d}c_{12}\int_0^1\mathrm{d}(\cos\theta)(1+e)\left[5+e-3(1+e)\cos^2\theta\right]\\
&\qquad\times\cos^3\theta c_{12}^7(693-297c_{12}^2+33c_{12}^4-c_{12}^6)\exp\left(-\tfrac{1}{2}c_{12}^2\right).
\end{aligned}\tag{B4c}$$

For $\beta v^* \to \infty$, these quantities reduce to

$$\omega_{\eta,1}^{e(\infty)} = -4 + (1-e^*)\left[(1-e^*)(1+x) - \tfrac{2}{3}(1+e^*)x^2\right]e^{-x}, \tag{B5a}$$

$$\omega_{\eta,2}^{e(\infty)} = \tfrac{1}{8} - \tfrac{1}{32}(1-e^*)\left[(1-e^*)(1+x) + 6(9+e^*)x^2 - 4(13+7e^*)x^3 + 8(1+e^*)x^4\right]e^{-x}, \tag{B5b}$$

$$\omega_{\eta,3}^{e(\infty)} = \tfrac{1}{32} - \tfrac{1}{128}(1-e^*)\left[(1-e^*)(1+x) + \tfrac{4}{3}(31+4e^*)x^2 - \tfrac{8}{3}(24+11e^*)x^3 + \tfrac{16}{3}(4+3e^*)x^4 - \tfrac{16}{9}(1+e^*)x^5\right]e^{-x}. \tag{B5c}$$

In a similar way, we derive Ω_κ^e defined by (2.14). Using the definition of $\tilde{\boldsymbol{S}}(\boldsymbol{c})$, (2.15), we write

$$\begin{aligned}
&\tilde{\boldsymbol{S}}(\boldsymbol{c}_2)\cdot\Delta\left[\tilde{\boldsymbol{S}}(\boldsymbol{c}_1)+\tilde{\boldsymbol{S}}(\boldsymbol{c}_2)\right] \\
&= \left(c_2^2 - \frac{5}{2}\right)\left[(\boldsymbol{c}_1'\cdot\boldsymbol{c}_2)c_1'^2 + (\boldsymbol{c}_2'\cdot\boldsymbol{c}_2)c_2'^2 - (\boldsymbol{c}_1\cdot\boldsymbol{c}_2)c_1^2 - (\boldsymbol{c}_2\cdot\boldsymbol{c}_2)c_2^2\right] \\
&= -\frac{1-e^2}{2}C^4(\boldsymbol{c}_{12}\cdot\hat{\boldsymbol{k}})^2 + \frac{1+e}{2}C^2c_{12}^2(\boldsymbol{C}\cdot\hat{\boldsymbol{k}})(\boldsymbol{c}_{12}\cdot\hat{\boldsymbol{k}}) - \frac{1-e^2}{8}C^2c_{12}^2(\boldsymbol{c}_{12}\cdot\hat{\boldsymbol{k}})^2 \\
&\quad - 2(1+e)C^2(\boldsymbol{C}\cdot\boldsymbol{c}_{12})(\boldsymbol{C}\cdot\hat{\boldsymbol{k}})(\boldsymbol{c}_{12}\cdot\hat{\boldsymbol{k}}) + \frac{(1+e)(5-3e)}{4}C^2(\boldsymbol{C}_{12}\cdot\boldsymbol{c}_{12})(\boldsymbol{c}_{12}\cdot\hat{\boldsymbol{k}})^2 \\
&\quad + (1+e)^2C^2(\boldsymbol{C}\cdot\hat{\boldsymbol{k}})^2(\boldsymbol{c}_{12}\cdot\hat{\boldsymbol{k}})^2 - \frac{(1+e)^2}{2}C^2(\boldsymbol{C}\cdot\hat{\boldsymbol{k}})(\boldsymbol{c}_{12}\cdot\hat{\boldsymbol{k}})^3 \\
&\quad + \frac{5(1-e^2)}{4}C^2(\boldsymbol{c}_{12}\cdot\hat{\boldsymbol{k}})^2 + \frac{1+e}{8}c_{12}^4(\boldsymbol{C}\cdot\hat{\boldsymbol{k}})(\boldsymbol{c}_{12}\cdot\hat{\boldsymbol{k}}) \\
&\quad - (1+e)c_{12}^2(\boldsymbol{C}\cdot\boldsymbol{c}_{12})(\boldsymbol{C}\cdot\hat{\boldsymbol{k}})(\boldsymbol{c}_{12}\cdot\hat{\boldsymbol{k}}) \\
&\quad + \frac{(1+e)(3-e)}{16}c_{12}^2(\boldsymbol{C}\cdot\boldsymbol{c}_{12})(\boldsymbol{c}_{12}\cdot\hat{\boldsymbol{k}})^2 + \frac{(1+e)^2}{4}c_{12}^2(\boldsymbol{C}\cdot\hat{\boldsymbol{k}})^2(\boldsymbol{c}_{12}\cdot\hat{\boldsymbol{k}})^2 \\
&\quad - \frac{(1+e)^2}{8}c_{12}^2(\boldsymbol{C}\cdot\hat{\boldsymbol{k}})(\boldsymbol{c}_{12}\cdot\hat{\boldsymbol{k}})^3 - \frac{5(1+e)}{4}c_{12}^2(\boldsymbol{C}\cdot\hat{\boldsymbol{k}})(\boldsymbol{c}_{12}\cdot\hat{\boldsymbol{k}}) \\
&\quad + 2(1+e)(\boldsymbol{C}\cdot\boldsymbol{c}_{12})^2(\boldsymbol{C}\cdot\hat{\boldsymbol{k}})(\boldsymbol{c}_{12}\cdot\hat{\boldsymbol{k}}) - \frac{(1+e)(3-e)}{4}(\boldsymbol{C}\cdot\boldsymbol{c}_{12})^2(\boldsymbol{c}_{12}\cdot\hat{\boldsymbol{k}})^2 \\
&\quad - (1+e)^2(\boldsymbol{C}\cdot\boldsymbol{c}_{12})(\boldsymbol{C}\cdot\hat{\boldsymbol{k}})^2(\boldsymbol{c}_{12}\cdot\hat{\boldsymbol{k}})^2 + \frac{(1+e)^2}{2}(\boldsymbol{C}\cdot\boldsymbol{c}_{12})(\boldsymbol{C}\cdot\hat{\boldsymbol{k}})(\boldsymbol{c}_{12}\cdot\hat{\boldsymbol{k}})^3 \\
&\quad + 5(1+e)(\boldsymbol{C}\cdot\boldsymbol{c}_{12})(\boldsymbol{C}\cdot\hat{\boldsymbol{k}})(\boldsymbol{c}_{12}\cdot\hat{\boldsymbol{k}}) - \frac{5(1+e)(3-e)}{8}(\boldsymbol{C}\cdot\boldsymbol{c}_{12})(\boldsymbol{c}_{12}\cdot\hat{\boldsymbol{k}})^2 \\
&\quad - \frac{5(1+e)^2}{2}(\boldsymbol{C}\cdot\hat{\boldsymbol{k}})^2(\boldsymbol{c}_{12}\cdot\hat{\boldsymbol{k}})^2 + \frac{5(1+e)^2}{4}(\boldsymbol{C}\cdot\hat{\boldsymbol{k}})(\boldsymbol{c}_{12}\cdot\hat{\boldsymbol{k}})^3.
\end{aligned} \tag{B6}$$

With (B2), (B6) and (2.14), we obtain

$$\Omega_\kappa^e \equiv \sqrt{2\pi}\left(\omega_{\kappa,1}^e + a_2\omega_{\kappa,2}^e + a_3\omega_{\kappa,3}^e\right), \tag{B7}$$

with

$$\omega^e_{\kappa,1} = \tfrac{1}{16}\int_0^\infty \mathrm{d}c_{12}\int_0^1 \mathrm{d}(\cos\theta)(1+e)\cos^3\theta c_{12}^5 \times\left[25(1-e)-(15-7e)c_{12}^2+4(1+e)\cos^2\theta c_{12}^2\right]\exp\left(-\tfrac{1}{2}c_{12}^2\right), \tag{B8a}$$

$$\omega^e_{\kappa,2} = \tfrac{1}{512}\int_0^\infty \mathrm{d}c_{12}\int_0^1 \mathrm{d}(\cos\theta)(1+e)\cos^3\theta c_{12}^5\exp\left(-\tfrac{1}{2}c_{12}^2\right) \times\left[175(1-e)+7(35+37e)c_{12}^2-(85+59e)c_{12}^4+(5+3e)c_{12}^6 -4(1+e)(63-18c_{12}^2+c_{12}^4)\cos^2\theta c_{12}^2\right], \tag{B8b}$$

$$\omega^e_{\kappa,3} = \tfrac{1}{6144}\int_0^\infty \mathrm{d}c_{12}\int_0^1 \mathrm{d}(\cos\theta)(1+e)\cos^3\theta c_{12}^5\exp\left(-\tfrac{1}{2}c_{12}^2\right) \times\left[-1575(1-e)+252(45-e)c_{12}^2-54(85+3e)c_{12}^4+4(125+7e)c_{12}^6 -(15+e)c_{12}^8-8(1+e)(693-297c_{12}^2+33c_{12}^4-c_{12}^6)\cos^2\theta c_{12}^2\right]. \tag{B8c}$$

For $\beta v^* \to \infty$, these quantities reduce to

$$\omega^{e(\infty)}_{\kappa,1} = -4-\tfrac{1}{8}(1-e^*)\left[(17+33e^*)(1+x)+22(1+e^*)x^2\right]e^{-x}, \tag{B9a}$$

$$\omega^{e(\infty)}_{\kappa,2} = -\tfrac{1}{8}+\tfrac{1}{256}(1-e^*) \times\left[(13-3e^*)(1+x)+2(67+3e^*)x^2-4(23+7e^*)x^3+8(1+e^*)x^4\right]e^{-x}, \tag{B9b}$$

$$\omega^{e(\infty)}_{\kappa,3} = -\tfrac{1}{16}+\tfrac{1}{1024}(1-e^*)\left[(11-21e^*)(1+x)+16(43+7e^*)x^2 -\tfrac{8}{3}(439+231e^*)x^3+\tfrac{16}{3}(79+63e^*)x^4-\tfrac{112}{3}(1+e^*)x^5\right]e^{-x}. \tag{B9c}$$

Appendix C. Numerical solution of the transport coefficients

Here, we provide some details of the numerical solution of the differential equations for the transport coefficients. Consider first the shear viscosity. Special care is in order since the corresponding differential equation (2.25*a*,*b*) is singular due to the fact that the coefficient of $\partial\eta^*/\partial x$ vanishes in both limits $x \to 0$ and $x \to \infty$.

Also the proper boundary conditions of this equation requires attention. In the high granular temperature limit all particles are expected to collide inelastically with one another, while in the limit of low granular temperature elastic interactions dominate. Thus, in the limit of high granular temperature, we expect the shear viscosity of a granular gas with coefficient of restitution e^*. For a low granular temperature, we expect to obtain the shear viscosity of a granular gas, corresponding to the coefficient of restitution 1. The proper boundary condition reads, therefore, as

$$\lim_{x\to 0}\eta^* = \frac{\eta^{(HC)}(e^*)}{\eta^{(HC)}(1)}, \tag{C1}$$

with

$$\eta^{(HC)}(e^*) \equiv \frac{15}{2(1+e^*)(13-e^*)\sigma^2}\sqrt{\frac{mT}{\pi}} \times \left[1+\frac{3(4-3e^*)}{8(13-e^*)}a_2^{(HC)}(e^*)+\frac{(7-4e^*)}{32(13-e^*)}a_3^{(HC)}(e^*)\right] \tag{C2}$$

(see also Brilliantov & Pöschel 2004).

For the numerical solution of (2.25*a*,*b*), we decompose the interval $x \in (0,\infty)$ into three intervals, (i) $x \in (0, e^{-1})$, (ii) $x \in [e^{-1}, e^{e/2})$ and (iii) $x \in [e^{e/2}, \infty)$.

In case (i) we introduce the new variable $y_1 \equiv \log x$ with $y_1 \in (-\infty, -1)$. Equation (2.25*a*,*b*) then reads as

$$10\mu_2^e e^{-e^{y_1}}\frac{\partial \eta^*}{\partial y_1} - \left(5\mu_2+6\Omega_\eta\right)\eta^* = 24\sqrt{2\pi}, \quad \text{with } \mu_2^e \equiv \mu_2 e^x, \tag{C3}$$

and the correspondingly boundary condition as

$$\lim_{y_1\to-\infty}\eta^* = \frac{\eta^{(HC)}(e^*)}{\eta^{(HC)}(1)}. \tag{C4}$$

In the next region (ii), we can directly solve (2.25*a*,*b*) since the coefficient of the derivative of η^* in (2.25*a*,*b*) is not small. The corresponding boundary condition reads as

$$\lim_{x\to e^{-1}+0}\eta^* = \lim_{x\to e^{-1}-0}\eta^*, \tag{C5}$$

where the right-hand side of this equation should be evaluated in terms of (C3). Finally, when considering region (iii), we introduce $y_2 \equiv e^x$ with $y_2 \in (e/2, \infty)$. Equation (2.25*a*,*b*) then reads as

$$10\mu_2^e \log y_2 \frac{\partial \eta^*}{\partial y_2} - \left(5\mu_2+6\Omega_\eta\right)\eta^* = 24\sqrt{2\pi}. \tag{C6}$$

In a similar way we solve numerically the differential equations (2.30) for the thermal conductivity and (2.31) for the coefficient μ. The corresponding boundary conditions read as

$$\lim_{x\to0}\kappa^* = \frac{\kappa^{(HC)}(e^*)}{\sqrt{T}}, \quad \lim_{x\to0}\mu^* = \frac{\mu^{(HC)}(e^*)}{\sqrt{T^{3/2}}}, \tag{C7a,b}$$

with

$$\kappa^{(HC)}(e^*) \equiv \frac{75}{2(1+e^*)(9+7e^*)\sigma^2}\sqrt{\frac{T}{\pi m}} \times \left[1+\frac{797+211e^*}{32(9+7e^*)}a_2^{(HC)}(e^*)+\frac{27-59e^*}{128(9+7e^*)}a_3^{(HC)}(e^*)\right], \tag{C8}$$

$$\mu^{(HC)}(e^*) \equiv \frac{750(1-e^*)}{(1+e^*)(9+7e^*)(19-3e^*)n\sigma^2}\sqrt{\frac{T^3}{\pi m}} \times \left[1+\frac{50\,201-30971e^*-7253e^{*2}+4407e^{*3}}{80(1-e^*)(19-3e^*)(9+7e^*)}a_2^{(HC)}(e^*) + \frac{459-646e^*-69e^{*2}}{64(19-3e^*)(9+7e^*)}a_3^{(HC)}(e^*)\right] \tag{C9}$$

(see also Brilliantov & Pöschel 2004).

References

Brey, J.J., Buzón, V., Maynar, P. & García de Soria, M.I. 2015 Hydrodynamics for a model of a confined quasi-two-dimensional granular gas. *Phys. Rev.* E **91**, 052201.

Brey, J.J. & Cubero, D. 2001 Hydrodynamic transport coefficients of granular gases. In *Granular Gases*, Granular gases edn. (ed. T. Pöschel & S. Luding), Lecture Notes in Physics, vol. 564, pp. 59–78. Springer.

Brey, J.J., Dufty, J.W., Kim, C.S. & Santos, A. 1998 Hydrodynamics for granular flow at low density. *Phys. Rev.* E **58**, 4638–4653.

Brey, J.J. & Ruiz-Montero, M. 2004 Simulation study of the Green–Kubo relations for dilute granular gases. *Phys. Rev.* E **70**, 051301.

Brey, J.J., Ruiz-Montero, M.J., Maynar, P. & García de Soria, M. 2005 Hydrodynamic modes, Green–Kubo relations, and velocity correlations in dilute granular gases. *J. Phys.: Condens. Matter* **17**, S2489.

Brilliantov, N.B., Salueña, C., Pöschel, T. & Schwager, T. 2004 Clustering and vortex formation as a transient process in granular gases. *Phys. Rev. Lett.* **93**, 134301.

Brilliantov, N.V. & Pöschel, T. 2000 Deviation from Maxwell distribution in granular gases with constant restitution coefficient. *Phys. Rev.* E **61**, 2809–2812.

Brilliantov, N.V. & Pöschel, T. 2003 Hydrodynamics and transport coefficients for dilute granular gases. *Phys. Rev.* E **67**, 061304.

Brilliantov, N.V. & Pöschel, T. 2006 Breakdown of the Sonine expansion for the velocity distribution of granular gases. *Europhys. Lett.* **74**, 424–430.

Brilliantov, N.V., Spahn, F., Hertzsch, J.-M. & Pöschel, T. 1996 Model for collisions in granular gases. *Phys. Rev.* E **53**, 5382.

Brilliantov, N.V. & Pöschel, T. 2004 *Kinetic Theory of Granular Gases*. Oxford University Press.

Chamorro, M.G., Reyes, F.V. & Garzó, V. 2013 Homogeneous steady states in a granular fluid driven by a stochastic bath with friction. *J. Stat. Mech.* P07013.

Dufty, J.W. & Brey, J. 2002 Green–Kubo expressions for a granular gas. *J. Stat. Phys.* **109**, 433–448.

Esipov, S.E. & Pöschel, T. 1997 The granular phase diagram. *J. Stat. Phys.* **86**, 1385.

Garzó, V. 2005 Instabilities in a free granular fluid described by the Enskog equation. *Phys. Rev.* E **72**, 021106.

Garzó, V. 2019 *Granular Gaseous Flows: A Kinetic Theory Approach to Granular Gaseous Flows*. Springer.

Garzó, V., Brito, R. & Soto, R. 2018 Enskog kinetic theory for a model of a confined quasi-two-dimensional granular fluid. *Phys. Rev.* E **98**, 052904.

Genareau, K., Wardman, J.B., Wilson, T.M., McNutt, S.R. & Izbekov, P. 2015 Lightning-induced volcanic spherules. *Geology* **43**, 319–322.

Goldhirsch, I. 2003 Rapid granular flows. *Annu. Rev. Fluid Mech.* **35**, 267–293.

Goldhirsch, I., Noskowicz, S.H. & Bar-Lev, O. 2003 The homogeneous cooling state revisited. In *Granular Gas Dynamics* (ed. T. Pöschel & N. Brilliantov), Lecture Notes in Physics, vol. 624, pp. 37–63. Springer.

Goldhirsch, I. & Zanetti, G. 1993 Clustering instability in dissipative gases. *Phys. Rev. Lett.* **70**, 1619.

Goldshtein, A. & Shapiro, M. 1995 Mechanics of collisional motion of granular materials. Part 1: general hydrodynamic equations. *J. Fluid Mech.* **282**, 75–114.

González, R.G. & Garzó, V. 2019 Transport coefficients for granular suspensions at moderate densities. *J. Stat. Mech.* **2019**, 093204.

Gupta, V.K., Shukla, P. & Torrilhon, M. 2020 Higher-order moment theories for dilute granular gases of smooth hard spheres. *J. Fluid Mech.* **836**, 451–501.

Haff, P.K. 1983 Grain flow as a fluid-mechanical phenomenon. *J. Fluid Mech.* **134**, 401–430.

JUNGMANN, F., STEINPILZ, T., TEISER, J. & WURM, G. 2018 Sticking and restitution in collisions of charged sub-mm dielectric grains. *J. Phys. Commun.* **2**, 095009.

KANAZAWA, S., OHKUBO, T., NOMOTO, Y. & ADACHI, T. 1995 Electrification of a pipe wall during powder transport. *J. Electrostat.* **35**, 47–54.

KOLEHMAINEN, J., OZEL, A., BOYCE, C.M. & SUNDARESAN, S. 2016 A hybrid approach to computing electrostatic forces in fluidized beds of charged particles. *AIChE J.* **62**, 2282–2295.

KUMAR, D., SANE, A., GOHIL, S., BANDARU, P.R., BHATTACHARYA, S. & GHOSH, S. 2014 Spreading of triboelectrically charged granular matter. *Sci. Rep.* **4**, 5275.

LACKS, D.J. & SHINBROT, T. 2019 Long-standing and unresolved issues in triboelectric charging. *Nat. Rev. Chem.* **3**, 465–476.

LAURENTIE, J.C., TRAORÉ, P. & DASCALESCU, L. 2013 Discrete element modeling of triboelectric charging of insulating materials in vibrated granular beds. *J. Electrostat.* **71**, 951–957.

LEE, V., WAITUKAITIS, S.R., MISKIN, M.Z. & JAEGER, H.M. 2015 Direct observation of particle interactions and clustering in charged granular streams. *Nat. Phys.* **11**, 733–737.

MURANUSHI, T. 2010 Dust-dust collisional charging and lightning in protoplanetary discs. *Mon. Not. R. Astron. Soc.* **401**, 2641–2664.

VAN NOIJE, T.P.C. & ERNST, M.H. 1998 Velocity distributions in homogeneous granular fluids: the free and the heated case. *Granul. Matt.* **1**, 57–64.

PAN, S. & ZHANG, Z. 2019 Fundamental theories and basic principles of triboelectric effect: a review. *Friction* **7**, 2–17.

PÖSCHEL, T. & BRILLIANTOV, N.V. (ed.) 2003 *Granular Gas Dynamics*, Lecture Notes in Physics, vol. 624. Springer.

PÖSCHEL, T., BRILLIANTOV, N.V. & SCHWAGER, T. 2003 Long-time behavior of granular gases with impact-velocity dependent coefficient of restitution. *Physica* A **325**, 274–283.

PUGLISI, A. 2015 *Transport and Fluctuations in Granular Fluids*, Springer Briefs in Physics, vol. 34. Springer.

SANTOS, A., GARZÓ, V. & DUFTY, J.W. 2004 Inherent rheology of a granular fluid in uniform shear flow. *Phys. Rev.* E **69**, 061303.

SANTOS, A. & MONTANERO, J.M. 2009 The second and third Sonine coefficients of a freely cooling granular gas revisited. *Granul. Matt.* **11**, 157–168.

SCHEFFLER, T. & WOLF, D.E. 2002 Collision rates in charged granular gases. *Granul. Matt.* **4**, 103–113.

SCHWAGER, T. & PÖSCHEL, T. 2008 Coefficient of restitution for viscoelastic spheres: the effect of delayed recovery. *Phys. Rev.* E **78**, 051304.

SELA, N. & GOLDHIRSCH, I. 1998 Hydrodynamic equations for rapid flows of smooth inelastic spheres, to Burnett order. *J. Fluid Mech.* **361**, 41–74.

SERERO, D. 2009 Kinetic theory of granular gas mixture. PhD thesis, Tel Aviv University.

SERERO, D., NOSKOWICZ, S.H., TAN, M.L. & GOLDHIRSCH, I. 2009 Binary granular gas mixtures: theory, layering effects and some open questions. *Eur. Phys.* J.*: Spec. Top.* **179**, 221–247.

SHUKLA, P., BISWAS, L. & GUPTA, V.K. 2019 Shear-banding instability in arbitrarily inelastic granular shear flows. *Phys. Rev.* E **100**, 032903.

SINGH, C. & MAZZA, M.G. 2018 Early-stage aggregation in three-dimensional charged granular gas. *Phys. Rev.* E **97**, 022904.

SINGH, C. & MAZZA, M.G. 2019 Electrification in granular gases leads to constrained fractal growth. *Sci. Rep.* **9**, 9049.

TAKADA, S. & HAYAKAWA, H. 2018 Rheology of dilute cohesive granular gases. *Phys. Rev.* E **97**, 042902.

TAKADA, S., SAITOH, K. & HAYAKAWA, H. 2016 Kinetic theory for dilute cohesive granular gases with a square well potential. *Phys. Rev.* E **94**, 012906.

TAKADA, S., SERERO, D. & PÖSCHEL, T. 2017 Homogeneous cooling state of dilute granular gases of charged particles. *Phys. Fluids* **29**, 083303.

WATANABE, H., GHADIRI, M., MATSUYAMA, T., DING, Y.L., PITT, K.G., MARUYAMA, H., MATSUSAKA, S. & MASUDA, H. 2007 Triboelectrification of pharmaceutical powders by particle impact. *Intl J. Pharm.* **334**, 149–155.

YOSHIMATSU, R., ARAÚJO, N.A.M., WURM, G., HERRMANN, H.J. & SHINBROT, T. 2017 Self-charging of identical grains in the absence of an external field. *Sci. Rep.* **7**, 39996.